Endogenous Chloride Channels of Insect *Sf*9 Cells

Evidence for Coordinated Activity of Small Elementary Channel Units

E. HVIID LARSEN, S.E. GABRIEL, M.J. STUTTS, J. FULLTON, E.M. PRICE, and R.C. BOUCHER

From the Cystic Fibrosis Center, Department of Medicine, University of North Carolina at Chapel Hill, Chapel Hill, North Carolina 27599-7020 and the August Krogh Institute, University of Copenhagen, DK-2100 Copenhagen Ø, Denmark

ABSTRACT The endogenous Cl^- conductance of *Spodoptera frugiperda* (*Sf*9) cells was studied 20–35 h after plating out of either uninfected cells or cells infected by a baculovirus vector carrying the cloned β-galactosidase gene (β-Gal cells). With the cation $Tris^+$ in the pipette and Na^+ in the bath, the reversal potential of whole-cell currents was governed by the prevailing Cl^- equilibrium potential and could be fitted by the Goldman-Hodgkin-Katz equation with similar permeabilities for uninfected and β-Gal cells. In the frequency range $0.12 < f < 300$ Hz, the power density spectrum of whole-cell Cl^- currents could be fitted by three Lorentzians. Independent of membrane potential, >50% of the total variance of whole-cell current fluctuations was accounted for by the low frequency Lorentzian ($f_c = 0.40 \pm 0.03$ Hz, $n = 6$). Single-Cl^- channels showed complex gating kinetics with long lasting (seconds) openings interrupted by similar long closures. In the open state, channels exhibited fast burst-like closures. Since the patches normally contained more than a single channel, it was not possible to measure open and closed dwell-time distributions for comparing single-Cl^- channel activity with the kinetic features of whole-cell currents. However, the power density spectrum of Cl^- currents of cell-attached and excised outside-out patches contained both high and low frequency Lorentzian components, with the corner frequency of the slow component ($f_c = 0.40 \pm 0.02$ Hz, $n = 4$) similar to that of whole-cell current fluctuations. Chloride channels exhibited multiple conductance states with similar Goldman-Hodgkin-Katz–type rectification. Single-channel permeabilities covered the range from $\sim 0.6 \cdot 10^{-14}$ cm^3/s to $\sim 6 \cdot 10^{-14}$ cm^3/s, corresponding to a limiting conductance ($\gamma_{150/150}$) of ~3.5 pS and ~35 pS, respectively. All states reversed near the same membrane potential, and they exhibited similar halide ion selectivity, $P_I > P_{Cl} \approx P_{Br}$. Accordingly, Cl^- current amplitudes larger than current flow through the smallest channel unit resolved seem to result from simultaneous open/shut events of two or more channel units. Key words: *Sf*9 cells • chloride channels • patch clamp • noise analysis • coordinated ion channel activity

INTRODUCTION

Expression of wild-type and engineered ion channel–forming proteins in immortalized cell lines constitutes an important tool for associating the chemical structure of the pore-forming molecule with biophysical properties of the conducting process such as gating, selectivity, conductance, rectification, and molecular pharmacology. The application of the cultured insect *Sf*9 cell line for heterologous expression of ion-channel proteins was introduced in Miller's laboratory in a study of *Shaker* potassium channels (Klaiber et al., 1990). It was demonstrated that by splicing the cloned foreign cDNA into the baculovirus vector, *Autographa californica*, and using the promoter of the viral polyhedron gene, high levels of the recombinant membrane protein could be expressed.

This expression system has been used now also for the study of anion selective channels, e.g., the cystic fi-

E.M. Price's current address is Dalton Research Center, Research Park, University of Missouri, Colombia, MO 65211.

Address correspondence to Erik Hviid Larsen, August Krogh Institute, Universitetsparken 13, DK-2100 Copenhagen Ø, Denmark. Fax: 45 3532 1567; E-mail:EHLarsen@aki.ku.dk

J. GEN. PHYSIOL. © The Rockefeller University Press • 0022-1295/96/06/695/20 $2.00
Volume 107 June 1996 695–714

brosis transmembrane conductance regulator (CFTR[1]; Kartner et al., 1991; Sarkadi et al., 1992; Gabriel et al., 1992), and of recombinant subunits of the human γ-aminobutyric acid receptor (Birnir et al., 1992; Nielsen et al., 1995). It has been advantageous for these studies that the heterologously expressed proteins could be studied superimposed upon small endogenous ion permeabilities. In our studies of *CFTR*-expressing *Sf*9 cells, however, it turned out that the baseline Cl^- permeability of *CFTR*-infected and uninfected cells was about the same (Larsen et al., 1992). Furthermore, single-channel studies indicated the presence of a small linear Cl^- channel (Gabriel et al., 1992) of a conductance similar to that reported for CFTR (Kartner et al., 1991; Bear et al., 1992). The gating kinetics of endogenous channels was complex, and single channels exibited very long dwell-times in open state, which also characterizes CFTR-mediated channel activity (Larsen et al., 1993; Fisher and Machen, 1994; Gadsby et al., 1995). We therefore determined that there was a need for a more thorough characterization of endogenous chloride channels of *Sf*9 cells, both at whole cell and at individual protein channel level. In the present study, we analyzed and compared properties of endogenous chloride channels by fluctuation analyses of macroscopic membrane currents and by single-channel recordings. Our results indicate that small elementary Cl^- channel units are found in close proximity to one another and that several units, transiently, exhibit coordinated gating. The resulting conductance transitions resemble the activity of larger channels. Furthermore, our results will aid further studies of the anion permeability of *Sf*9 cells after expression of anion transporters like, for example, CFTR and γ-aminobutyric acid receptor subunits.

MATERIALS AND METHODS

Preparation

We used cultured insect *Spodoptera frugiperda* (*Sf*9, InVitrogen Corp., San Diego, CA) cells, uninfected or infected with recombinant virus carrying the β-galactosidase gene. Infected cells were included to investigate whether expression of viral proteins influences the magnitude of endogenous whole-cell chloride conductance. The cells were maintained at 27°C in Petri dishes (Nunc, Roskilde, Denmark; 4 cm OD, 2 ml, $3 \cdot 10^6$ cells/ml) in Grace's medium supplemented with yeastolate and lactalbumin hydrolysate, to which we added 10% fetal bovine serum and antibiotics (50 μg/ml gentamycin). Electrophysiological recordings were made at room temperature between 20 and 35 h after plating and replacing of the tissue-culture medium with either of the bath solutions indicated below ("Solutions"). Practically all cells retained their original spherical shape during incubation as well as during the subsequent patch-clamp studies.

Whole-Cell and Single-Channel Current Recordings

Patch pipettes were constructed from borosilicate glass tubes with an inner filament (GC150F; Clark Instruments, Reading, UK) on a Narishige PP-83 or a DMZ (Zeitz Instruments, Augsburg, Germany) patch electrode puller using standard two-pull and three-pull techniques, respectively. The tip was heat polished to give an electrode resistance of 2–3 MΩ when measured with the respective standard solutions in electrode and culture dish, respectively (see "Solutions"). The culture dish was positioned on the table of an inverted microscope (IM35; Carl Zeiss, Inc., Thornwood, NY), and the cells were viewed with DIC Nomarski optics at a magnification of 500. With a small pressure applied to the pipette solution, the tip of the patch pipette was directed with a three-dimensional hydraulic micromanipulator (MO-103; Narishige, Tokyo, Japan) to the surface of a selected cell. All four variants of the patch-clamp methods were used (Hamill et al., 1981). Whole-cell recording conditions were obtained by suction (~−0.2 atm) applied to cell-attached patches with a membrane-pipette seal-resistance >30 GΩ. Excised outside-out patches were formed from the whole-cell configuration by slow withdrawal of the pipette.

After giga-seal formation, patch-electrode voltage clamps and current recordings were performed with an RK-300 amplifier (Biologic, Claix, France) furnished with a headstage feedback resister of either 100 MΩ (whole-cell recordings) or 10 GΩ (single-channel recordings). The CED patch- and voltage-clamp software and the CED 1401 interface were used for generating clamping programs and acquiring, digitizing, and analyzing resulting currents (Cambridge Electronic Design, Cambridge, UK). Single-channel currents were recorded to videotape (modified PCM-501ES, Sony Tokyo; AG-6200, Panasonic, Osaka, Japan) and subsequently low-pass filtered (f_c[−3 dB] = 200–1,000 Hz; eight-pole Bessel, or eight-pole Butterworth when indicated [see Fig. 14]; Frequency Devices, Inc., Haverhill, MA) and digitized at 1 or 2 kHz. In some but not all experiments, capacitance neutralizations were performed. Because of the small membrane currents of *Sf*9 cells, the pipette access resistance was not always corrected for.

Current Processing for Fluctuation Analyses

Current fluctuations were analyzed according to standard methods (Anderson and Stevens, 1973; Lindemann and Van Driessche, 1978) using the SPAN program of Dempster's patch- and voltage-clamp software package (Strathclyde Electrophysiology, Glasgow, UK). For obtaining power density spectra (PDS) of sufficient resolution and at the same time covering the considerable range of 0.12–1,000 Hz, it was necessary to process, with different bandwidth and time record length, the same stationary current segment twice: Stationary whole-cell currents of 150–180 s duration stored on videotape were low-pass filtered (−3 dB, eight-pole Bessel) at 990 Hz or 245 Hz and digitized at an amplification of 10 at a sampling rate of 2,000 Hz or 500 Hz, respectively. The high and low frequency spectra were then calculated by a 4,096-point fast Fourier transform over square-pulse time windows covering 2.048-s or 8.192-s current records, respectively. Each spectrum was obtained by averaging such 16–180 individually transformed records and merged to a single PDS before curve fitting. Some

[1]*Abbreviations used in this paper.* CFTR, cystic fibrosis transmembrane conductance regulator; GHK, Goldman-Hodgkin-Katz; PDS, power density spectrum.

spectra were also calculated by multiplying the fast Fourier transforms with a 10% cosinus bell window time function, but the results obtained were not significantly affected by this type of windowing (not shown). Generally, therefore, fast Fourier transformations were performed without multiplying with any time window function. All spectra are shown and were analyzed without notch-filtering. Two to three Lorentzian curves (see Eq. 7a) were fitted to the calculated PDS using the Levenberg-Marquardt nonlinear least-square routine. The stationary mean-current component used for calculating the variance of fluctuations (see Eq. 5b) was obtained by additional sampling and digitizing through a low-gain (×1) DC-coupled channel.

Intracellular Potentials of Sf9 Cells

During the first day of incubation, *Sf*9 cells settled on the bottom of the Petri dish, and they could be impaled with a conventional single-barreled microelectrode (2 M KCl filling solution, 80–120 MΩ tip resistance) connected to a high impedance electrometer (N-707A; World Precision Instruments, Inc., Sarasota, FL) and using a piezo-electric transducer (PM20H; Elke Nagel-Biomedizinische Instrumente, München, Germany) for advancing the tip of the electrode through the membrane of a visually selected cell. With standard bath outside (150 mM Cl^-, see below), intracellular potentials ranged from −10 to −25 mV with a mean value, $V_C = -14.2 \pm 4.9$ mV (±SEM, $n = 10$ cells). With the likely assumption that Cl^- is in equilibrium (see below), implying that at steady state the membrane potential is set by the distribution of the small diffusible cations and their respective membrane permeabilities, the above value of V_C would indicate an intracellular Cl^- concentration of ~80 mM.

Solutions

Standard bath solution contained the following(mM): 127 Na^+, 4 Ca^{2+}, 5 Mg^{2+}, 150 Cl^-, 10 glucose, 50 mM sucrose, and 10 *N*-tris (hydroxymethyl) methyl-2-aminoethane sulfonic acid (TES), pH = 6.8. In sodium-free bathing solution, Na^+ was replaced by $Tris^+$. Standard pipette solution contained the following (mM): 130 $Tris^+$, 0.8 Mg^{2+}, 0.38 Ca^{2+} + 1 mM EGTA (100 nM free Ca^{2+}), 40 Cl^-, 90 gluconate, 3 ATP, 0.1 ADP, 0.05 GTP, 1 pyruvate, 1 acetate, 1 L-aspartate, 1 D-glucose, 5 TES, pH = 7.2 adjusted with NaOH resulting in a final $[Na^+]$ of 12 mM. In experiments with pipette $[Cl^-]$ raised to 140 mM, $Tris^+$ was raised to 140 mM and added as Tris-HCl.

Channel selectivity studies were performed with Br^- or I^- partially replacing Cl^- in the bath: 100 mM of either Br^- or I^-, 50 mM Cl^-, otherwise identical to the standard bath solution indicated above. 10 mM of either NaBr or NaI was added to standard pipette solution (above), maintaining $[Cl^-]_P = 40$ mM. Only reagent-grade chemicals were used.

Correction for Liquid Junction Potentials

With the pipette in the bath, the liquid junction potential (V_{LJ}) between the bath and pipette solutions as well as other external electromotive forces was nulled before the pipette tip was pressed against a selected cell. Thus, in cell-attached recordings with different solutions in bath and pipette ($V_{LJ} \neq 0$), and with pipette potential, V_P, the patch-membrane potential (V_M) becomes (Neher, 1991)

$$V_M = V_C - V_P + V_{LJ}. \tag{1a}$$

Here, V_C is the intracellular potential (cf. above), and V_{LJ} indicates bath potential relative to pipette potential. With similar conventions, in the whole-cell and excised outside-out configurations, V_M is given by:

$$V_M = V_P - V_{LJ}. \tag{1b}$$

V_{LJ} for bath/pipette solution pairs used in the present study was measured with floating 2 M KCl bridges and large solution reservoirs. The values obtained are listed in Table I.

TABLE 1

Liquid Junction Potentials of Bath/Pipette Solution Pairs

Bath solution*	Pipette solution*	V_{LJ}‡
150 mM Cl^-	40 mM Cl^-	+8.0 mV
50 mM Cl^-/100 mM Br^-	40 mM Cl^-/10 mM Br^-	+6.3 mV
50 mM Cl^-/100 mM I^-	40 mM Cl^-/10 mM I^-	+5.8 mV

The values are means of three to five determinations which, with the floating KCl bridges and large solution reservoirs, showed practically no variation among subsequent measurements.

*Only halide ion concentrations are listed. Other components are listed in Materials and Methods.

‡The sign convention of V_{LJ} is such that bath potential is given relative to pipette potential.

Description of Ion Flow through Chloride Channels

It turned out that the Cl^- current–voltage relationship of a homogenous constant field membrane could be fitted to currents obtained from both whole-cell and single-channel voltage-clamp recordings. The current, i_{Cl}, carried by such a channel obeys the Goldman-Hodgkin-Katz (GHK) current equation (Goldman, 1944; Hodgkin and Katz, 1949):

$$i_{Cl} = \frac{P_{Cl} \cdot F^2 \cdot V \cdot \{[Cl^-]_c - [Cl^-]_o \cdot \exp(-F \cdot V/(R \cdot T))\}}{R \cdot T \cdot \{1 - \exp(-F \cdot V/(R \cdot T))\}}, \tag{2}$$

where P_{Cl} is the single-channel permeability (cm^3/s per channel), V is the membrane potential with reference to external bath, $[Cl^-]$ denotes concentration on the external (o) and internal (c) side of the membrane, and F, R, and T have their usual meanings. The integral (or chord) conductance (γ_{Cl}) of the channel is given by the following (e.g., Finkelstein and Mauro, 1963; Sten-Knudsen, 1978):

$$\gamma_{Cl} = \frac{P_{Cl} \cdot F^3 \cdot V \cdot \{[Cl^-]_c - [Cl^-]_c \cdot \exp(-F \cdot V/(R \cdot T))\}}{R^2 \cdot T^2 \cdot \{\exp(-F \cdot V/(R \cdot T)) - 1\} \cdot \ln\{[Cl^-]_c/\langle [Cl^-]_c \cdot \exp(-F \cdot V/(R \cdot T))\rangle\}} \quad (V \neq E)_{Cl} \tag{3a}$$

$$\gamma_{Cl} = \frac{P_{Cl} \cdot F^3 \cdot V \cdot [Cl^-]_o \cdot [Cl^-]_c}{R^2 \cdot T^2 \cdot \{[Cl^-]_o - [Cl^-]_c\}} \quad (V = E_{Cl}) \quad (3b)$$

with $i_{Cl} = \gamma_{Cl} \cdot (V - E_{Cl})$, and the equilibrium potential, $E_{Cl} = -(R \cdot T/F) \cdot \ln([Cl^-]_o / [Cl^-]_c)$. In symmetrical 150-mM Cl^- solutions, a condition often prevailing in studies of excised inside-out patches, the channel conductance would be given by:

$$\gamma_{150/150} = \frac{P_{Cl} \cdot F^2 \cdot [Cl^-]}{R \cdot T} \quad ([Cl^-] = 150 \text{ mM}). \quad (3c)$$

In the text, $\gamma_{150/150}$ denotes the limiting conductance. Halide ion selectivity of single channels studied in the outside-out patch configuration was estimated from the channel's reversal potential, V_r, in experiments with mixtures of Cl^- and another halide ion, $A = Br^-$ or I^-, in both bath and pipette solution. The relative permeability, P_A/P_{Cl}, was calculated by the following equation derived from the GHK potential equation:

$$\frac{P_A}{P_{Cl}} = \frac{[Cl^-]_o - [Cl^-]_c \cdot \exp(-V_r \cdot F/(R \cdot T))}{[A]_c \cdot \exp(-V_r \cdot F/(R \cdot T)) - [A]_o} \quad (4)$$

where V_r is the reversal potential corrected for the liquid junction potential (cf. above). Whole-cell currents, I_{Cl}, were also fitted by Eq. 2, providing the chloride permeability of the cell membrane (cm^3/s per cell), which entered into Eqs. 3a and 3b for calculating the associated macroscopic Cl^- conductances (G_{Cl}).

Interpretation of Stationary Current Fluctuations

Noise data were analyzed in terms of their variance, σ^2, and power spectral densities, $S(f)$, where σ^2 was obtained by integrating the theoretical (fitted) PDS (Christensen and Bindslev, 1982; Lindemann, 1984):

$$\sigma^2 = \int_0^\infty S(f) \cdot df \quad (5a)$$

or calculated from the digitized current fluctuations constrained by the external low-pass filtering:

$$\sigma^2 = \Sigma (I_m - I_j)^2/(n-1) \text{ over the interval, } 1 \le j \le n, \quad (5b)$$

where I_m is the mean current, and n is the number of digitized current data, I_j, entering the calculation.

Extraneous noise sources. Whole-cell current noise contains unavoidable error components like the intrinsic white noise (S_{th}^2) generated by current flow in the headstage feedback resistor (R_f):

$$S_{th}^2 = 4k \cdot T/R_f, \quad (6a)$$

and the frequency dependent noise contributed by the serial configuration of membrane capacitance, C_M, and access resistance, R_A (Marty and Neher, 1995):

$$S(f) = \frac{4k \cdot T \cdot R_A \cdot (2\pi \cdot f \cdot C_M)^2}{1 + (2\pi \cdot f \cdot R_A \cdot C_M)^2}, \quad (6b)$$

with $k = 1.38 \cdot 10^{-23}$ J · K^{-1}, $T = 293$ K, and $R_f = 10^8$ Ω (whole-cell recordings), $S_{th}^2 = 1.6 \cdot 10^{-4}$ pA^2/Hz. The "noise floor" of the patch-clamp station was measured with the pipette holder mounted on the headstage and with the electrode in air (mechanical and thermal noise sources and noise from the tape recorder on which the data were temporarily stored), and this was compared with the Johnson-Nyquist noise of the feedback resistor (Eq. 6a). In the frequency range, $2 < f < 1{,}000$ Hz, the background noise contributed by the work station was independent of frequency and given by the thermal power spectrum of the headstage's feedback resistor (Fig. 1). Below this range, in the absence of current flow, excess noise becomes visible, which here (but see also Fig. 3) resembles "$(1/f)$-noise" superimposing power spectra of current fluctuations of some (Poussart, 1971; Fishman, 1973; DeFelice, 1981; Lindemann and Van Driessche, 1978; Van Driessche and Zeiske, 1985), but not all (Conti et al., 1980; Larsen and Harvey, 1994), biological whole-cell preparations. The passive circuit (Fig. 1, *inset*) simulates an *Sf*9 cell in whole-cell recording mode. The power spectrum was obtained by driving, with a holding potential of 200 mV, a DC current of 970 pA to ground. Also, in this situation the noise power spectrum is white over a considerable range of frequences with vanishingly small low frequency excess noise added to that measured in the absence of current flow. The noise generated by the R_AC_M network was calculated from Eq. 6b, and in the higher frequency range this theoretical spectrum merges nicely with the PDS of the model circuit actually measured. Finally, Fig. 1 also depicts the

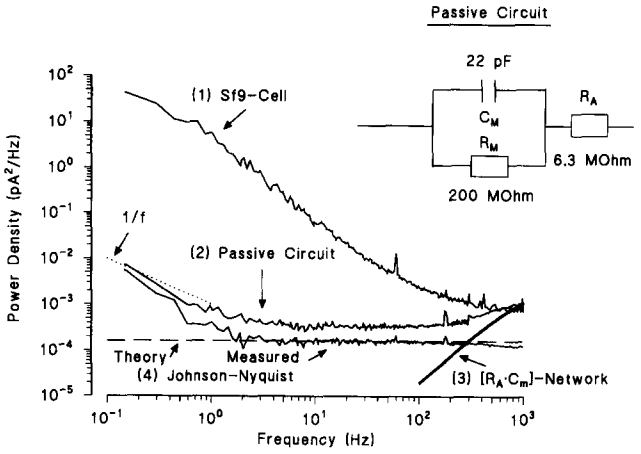

FIGURE 1. Power spectra of extraneous noise sources compared with that of fluctuations in whole-cell currents recorded from an uninfected *Sf*9 cell. Each experimental spectrum was obtained by sampling blocks of 4,096 data points of a 160-s stationary current segment as explained in Materials and Methods. (*1*) The *Sf*9 spectrum was obtained by driving 600 pA from cell to bath in whole-cell voltage-clamp mode. (Inset) The passive network of a 22-pF capacitor (C_M) in parallel with a 200-MΩ resister (R_M) models a *Sf*9 cell with surface area of $\sim 2 \cdot 10^{-5}$ cm^2 and with a specific membrane resistance of ~ 4 KΩ · cm^2 (5 nS/cell). The network's serial access resistance, R_A = 6.3 MΩ, simulates a 2–3-MΩ patch electrode (measured in free solution) in the whole-cell configuration. Its experimental noise spectrum (*2*) was generated with the network mounted on the headstage and a 970-pA DC current flowing to ground. The high frequency power of the experimental spectrum should be compared with that calculated from Eq. 6b in the text and shown as spectrum *3*. The background noise spectrum (*4, Measured*) was recorded with a patch pipette mounted on the headstage and with the tip in air; the spectrum should be compared with that calculated from Eq. 6a and indicated by the dashed line (*4, Theory*).

noise power spectrum of whole-cell current fluctuations sampled from an *Sf*9 cell ($E_{Cl} = -33$ mV, $V_p - E_{Cl} = 60$ mV, $I_m = 600$ pA). There is a small 60-Hz noise peak and its higher harmonics superimposed on the *Sf*9 cell noise spectrum, and, as expected for $f > 300$ Hz, the unavoidable noise contributed by the recording network is also evident.

Biological noise sources. For a single population of channels exhibiting stochastic behavior, the PDS of macroscopic current fluctuations, caused by random open/shut events of individual channels, is given by the following (Stevens, 1972; Neher and Stevens, 1977; Colquhoun and Hawkes, 1977):

$$S(f) = \frac{S_0}{1 + (f/f_c)^2}, \tag{7a}$$

where S_0 is the low frequency asymptote, and the corner frequency, f_c, is related to the time constant (τ) of the fluctuations by:

$$f_c = 1/(2\pi \cdot \tau). \tag{7b}$$

Accordingly, with N channels having open probability, p_o, and carrying current, i, in its open state of mean duration, τ^{open}, we have (e.g., Neher and Stevens, 1977):

$$I_m = i \cdot p_o \cdot N \tag{8a}$$

$$i = \sigma^2/[I_m \cdot (1 - p_o)] \tag{8b}$$

$$\tau^{open} = \tau/(1 - p_o), \tag{8c}$$

where I_m is the mean whole-cell current. Performing the integration in Eq. 5a, with $S(f)$ defined by Eq. 7a, it follows that the bandwidth-unlimited variance entering into Eq. 8b can be calculated from:

$$\sigma^2 = \pi \cdot S_0 \cdot f_c/2. \tag{9}$$

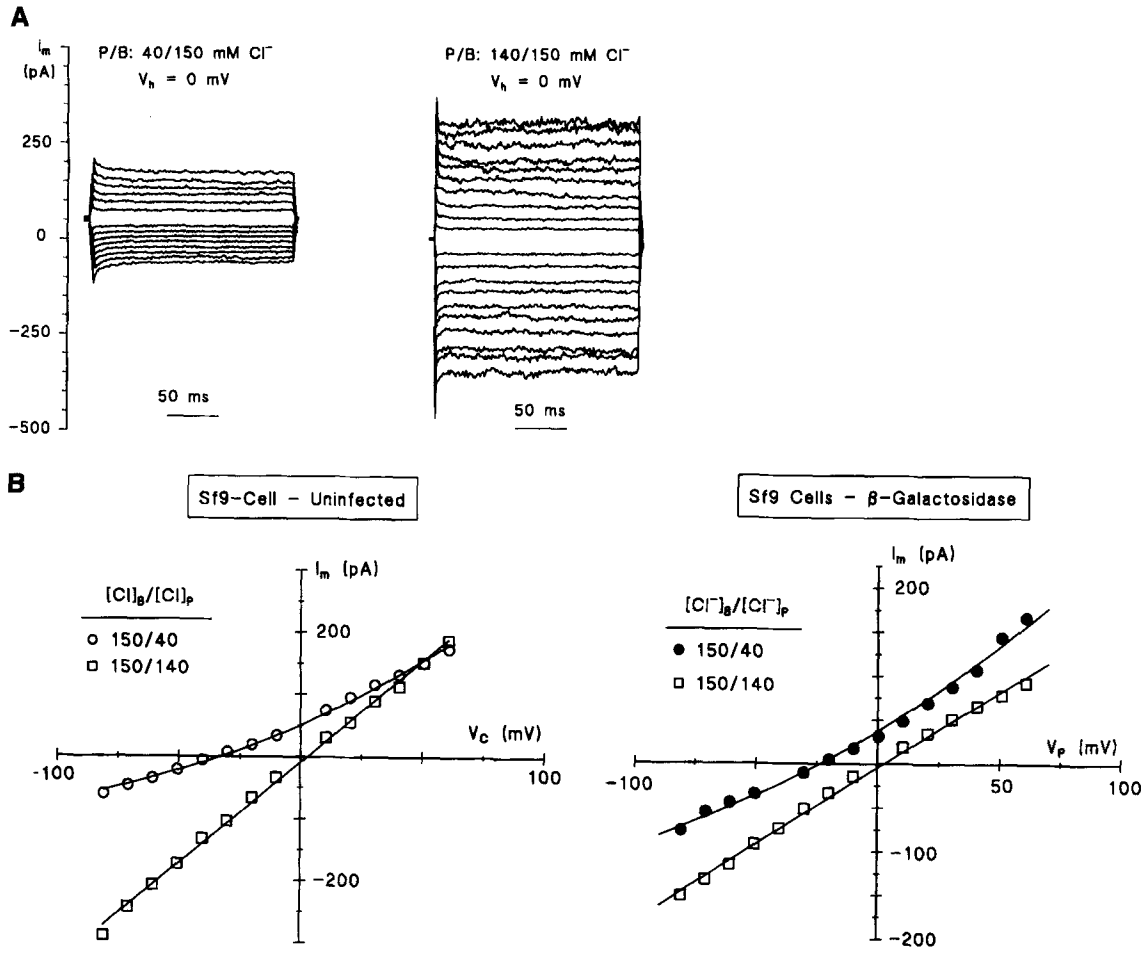

FIGURE 2. Whole-cell currents of *Sf*9 cells. (*A*) Uninfected cells. Shown are current responses to 200-ms square voltage pulses generated from 0 mV holding potential and with pulse amplitude varying in steps of 10 mV from −80 to +60 mV. Currents were filtered at 500 Hz and digitized at 1-ms intervals. (*Left*) With pipette/bath $[Cl^-]$ = 40/150 mM, the membrane rectified in the outward direction; outward currents were more noisy. (*Right*) With pipette/bath $[Cl^-]$ = 140/150 mM, current amplitudes were near-symmetrical for voltage steps of similar amplitude and opposite signs, and the noisy appearance no longer depended on direction of current flow. (*B*) *I/V* relationships constructed from currents generated in the way shown in *A* by sampling from 150 to 190 ms after onset of voltage pulse. Raising $[Cl^-]_p$ from 40 to 140 mM resulted in rightward displacement of reversal potential towards zero, as expected for currents carried predominantly by chloride. The full lines show the fit of Eq. 2 to experimental data.

TABLE II

Membrane Currents of Sf 9 Cells, Uninfected or Expressing Recombinant cDNA from the Baculovirus Vector, Autographa californica

Cells	V_r	V_r^{corr}	P_{Cl}	G_r	n
	mV		*10^{-12} cm³/(s·cell)*	*pS/cell*	
Uninfected	−34.1 ± 2.0	−42.1	2.4 ± 0.3	644 ± 100	13
β-Galactosidase	−31.7 ± 2.1	−39.7	2.4 ± 0.5	608 ± 96	12

V_r is the reversal potential obtained from current–voltage curves as indicated in Fig. 2. V_r^{corr} is the reversal potential corrected for liquid junction potential, V_{LJ} (=8 mV, Table I). With bath [Cl^-] = 150 mM and pipette [Cl^-] = 40 mM, the calculated E_{Cl} = −33.4 mV. G_r is the cell membrane conductance at the reversal potential calculated by Eq. 3b.

Data Presentation

Mean values of all-point Gaussian distributions of digitized currents are given with their standard deviation (± SD). Unless otherwise indicated (see Fig. 3), other mean values are given with their standard error (± SEM), with n indicating the number of observations.

RESULTS

Macroscopic Membrane Conductance of Sf9 Cells

With the cation $Tris^+$ in the pipette, Na^+ in the bath, and pipette/bath [Cl^-] = 40/150 mM, the whole-cell currents in uninfected and β-galactosidase (β-Gal)–infected *Sf*9 cells rectified as expected for a Cl^- current (Eq. 2, Fig. 2, *A* and *B*). However, the reversal potential (corrected for liquid junction potential; see Table II) was somewhat more negative than the chloride equilibrium potential. With pipette [Cl^-] raised to 140 mM, the *I/V* relationships became near-linear (Fig. 2, *A* and *B*) and had the following reversal potentials: −1.4 ± 0.6 mV (n = 12 uninfected cells) and −2.0 ± 2.0 mV (n = 11 β-Gal cells), respectively. These results provide the evidence that the major membrane current is carried by chloride ions, and they support the conclusion that *Sf*9 cells express a significant endogeneous chloride permeability as reported in a previous single-channel study (Gabriel et al., 1992). Notably, the spontaneous endogenous chloride permeability could not be further increased by forskolin: P_{Cl} = 2.8 (± 1.4) · 10^{-12} cm³/(s · cell) before forskolin treatment; P_{Cl} = 2.3 (± 0.8) · 10^{-12} cm³/(s · cell) 5 min after the addition of 25 μM forskolin to bath, ΔP_{Cl} = −0.5 (± 0.9) · 10^{-12} cm³/(s · cell) for paired observations (n = five cells; the ΔP_{Cl}^- value is not significantly different from zero).

Variance and PDS of Current Fluctuations

Fig. 3 *A* shows stationary current fluctuations generated by native insect channels carrying a current from cell to bath. The mean membrane current, and the associated variance of the fluctuations calculated according to Eq. 5b, are indicated on the respective recordings. Shifting the driving force for current flow from +50 mV to near E_{Cl} resulted in a reduction of the membrane current from 223 to 6.5 pA and a drop in variance from 16 to 0.39 pA². The latter σ^2 value is no more than 2.5 times above the variance of the thermal noise fluctuations produced by the 100 MΩ feedback resister of the headstage (0.16 pA²; calculated from Eq. 6a for a band, Δf = 989 Hz). This finding permits the conclusion that the much larger fluctuations recorded at $V_c \neq E_{Cl}$ are caused, predominantly, by random open/shut events of chloride channels. This important point is discussed in further detail in connection with our single-channel current recordings, presented below.

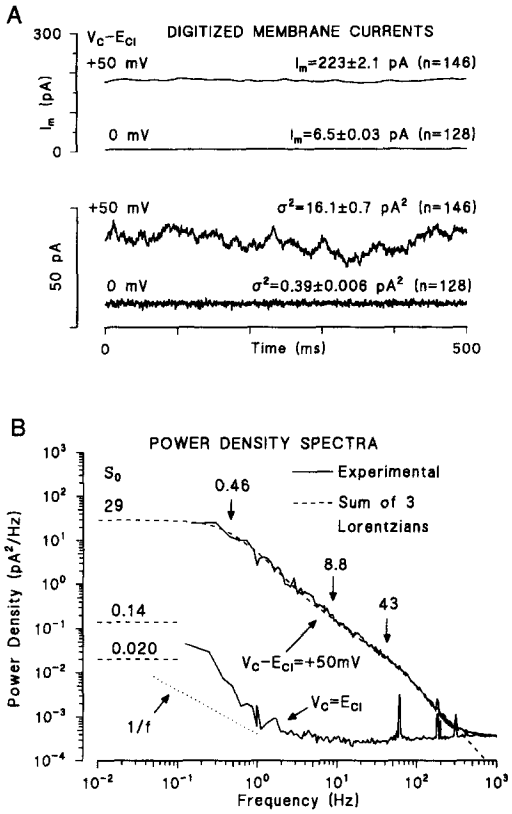

FIGURE 3. (*A*) Membrane currents digitized at low gain and narrow, 50-Hz bandwidth and high gain and 990-Hz bandwidth. The two sets of currents were obtained with a 50-mV inward driving force on chloride ions, and with pipette potential clamped near E_{Cl} (nominally equal to −33 mV; $[Cl^-]_P$ = 40 mM), respectively. Mean currents and variances (± SD) are shown above each trace, with n the number of 1-s records. As indicated by the small SDs, requirements of stationary conditions were reasonably well fulfilled. (*B*) PDS of currents carried by an outward flux of Cl^- constructed as explained in the legend of Fig. 1. The dashed line is the fit of the sum of three Lorenzians in the frequency range, 0.12–250 Hz (Eq. 7a), with their respective cutoff frequencies (f_c, *arrows*) and low-frequency asymptotes (S_0, *stipled lines*) indicated by the numbers. It should be noted that the variances obtained in *A* are based on 1-s records. Thus, these values of σ^2 underestimate the variances that can be calculated from the PDS shown in *B* (record length 8 s).

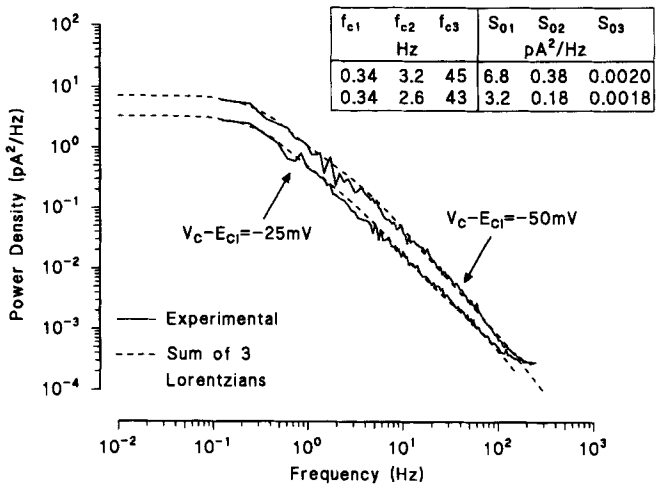

FIGURE 4. PDS of currents carried by an outward flux of chloride ions (i.e., current direction from bath to cell). Fitted parameters of three Lorentzians (*inset*) with their sum are shown as a dashed line superimposed upon each experimental spectrum.

As already indicated in Fig. 1, PDS calculated from current flowing from cell to bath through the *Sf*9 cell membrane contains several corner frequencies. The two spectra obtained from current fluctuations shown in Fig. 3 *A* are depicted in Fig. 3 *B*. A good fit to the experimental spectrum, calculated for $V_C \neq E_{Cl}$, was obtained with three Lorentzian components. Fig. 4 shows that Cl^- currents flowing in opposite directions, from bath to cell, exhibited a similar complex PDS. Admittedly, the two higher corner frequencies showed a considerable variation from preparation to preparation, reflecting the fact that the fitting of three Lorentzian components (with six parameters) is statistically difficult. It was a consistent finding, however, that the spectrum always contains a low frequency component (f_{c1} = 0.3–0.5 Hz), indicating that a slowly gated population of Cl^- channels contributes significantly to the variance of the macroscopic current fluctuations. This is the point we want to emphasize here, and it is clearly illustrated by the summarizing data given in Table III, which contains parameters of fitted Lorentzian components at driving forces ranging from −60 mV to +50 mV. For outward as well as for inward chloride ion flows, more than half (between 63 and 92%; Table III) of the variance is associated with a low frequency Lorentzian component. This finding is consistent with the hypothesis that chloride current fluctuations are predominantly governed by a population of channels with a relaxation time constant, 325 ms $< \tau <$ 550 ms, where $\tau = 1/2\pi f_c$. With an open probability between 0.2 and 0.8, we would predict for such slow channel

TABLE III

Estimated Macroscopic Gating Kinetics of Endogenous Chloride Channels in Insect Sf9 Cells

$V_p - E_{Cl}$	f_1	f_2	f_3	S_1	S_2	S_3	σ_1^2	σ_2^2	σ_3^2
mV		s^{-1}			pA^2s			pA^2	
−60	0.29	12.5	120	37.4	0.10	0.010	17.0	1.96	1.88
−50	0.34	3.2	45	6.8	0.38	0.002	3.63	1.91	0.14
−25	0.34	2.6	43	3.2	0.18	0.002	1.71	0.74	0.13
+25	0.49	9.1	44	14	0.02	0.010	10.8	0.29	0.69
+40	0.48	41.3	185	88	0.13	0.098	66.4	8.43	28.4
+50	0.45	8.8	43	29	0.14	0.020	20.5	1.93	1.35

The estimated corner frequencies and low frequency asymptotes were obtained by fitting three Lorentzian components to difference spectra; *i.e.*, for each experiment the power density spectrum calculated at $V_p - E_{Cl} \cong 0$ mV was subtracted from the power density spectrum obtained at the potential indicated in first column.

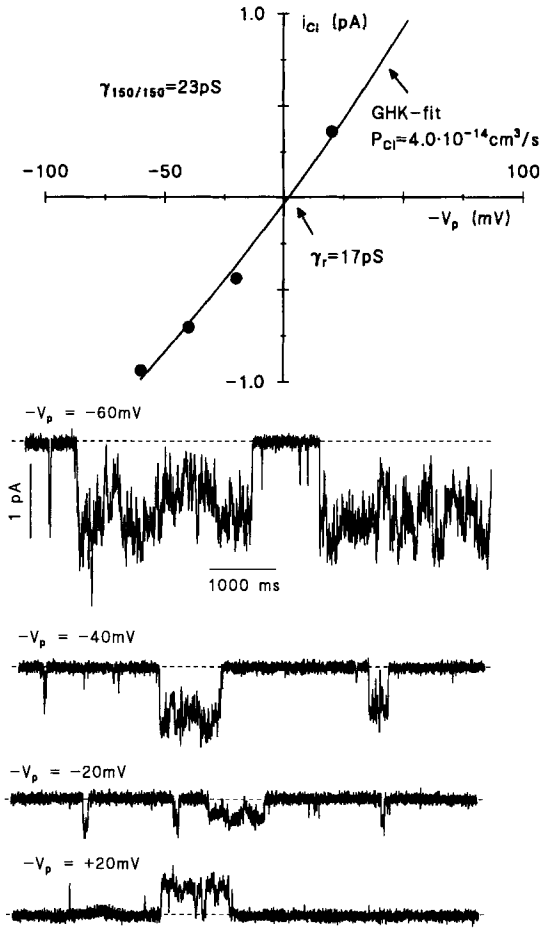

FIGURE 5. Cell-attached patch recordings of an endogenous chloride channel of *Sf*9 cell. Similar solutions in bath and pipette with $[Cl^-]$ = 150 mM. The four recordings are shown with similar gain and time scale. They were obtained at pipette potentials indicated above the traces. The *i/V* relationship was constructed from the means of Gaussian fits to amplitude distribution histograms of digitized current points. The full line is the fit of Eq. 2 with P_{Cl} = $4.0 \cdot 10^{-14}$ cm³/s, $[Cl^-]_C$ = 88 mM, and V_C = −13.4 mV. γ_{rev} = 17 pS and $\gamma_{150/150}$ = 23 pS were calculated by Eqs. 3b and 3c, respectively. R_{seal} = 57 GΩ.

transitions a rather long mean open time, $0.4\ s < \tau^{open} < 2.5\ s$ (Eqs. 8, 9). It follows that the two higher frequency Lorentzian components would then be associated (*a*) with additional electrical activity of this population of channels, such as burst-like activity (Colquhoun and Hawkes, 1977); or (*b*) with independent activity of other populations of channels exhibiting, on the average, open and closed times of shorter durations. To explore these possibilities, we performed single-channel current recordings.

Single-Channel Recordings from Cell-attached Patches

Within the first 20–35 h after plating, neither infected nor uninfected *Sf*9 cells were difficult to patch, and membrane pipette seals of 50–200 GΩ were easily obtained. Seals often remained stable for 30 min or more. If channel activity was not recorded within the first 5 min after seal formation, it was concluded that the patched membrane did not contain electrically active channels. Using this criterion, we resolved channels in

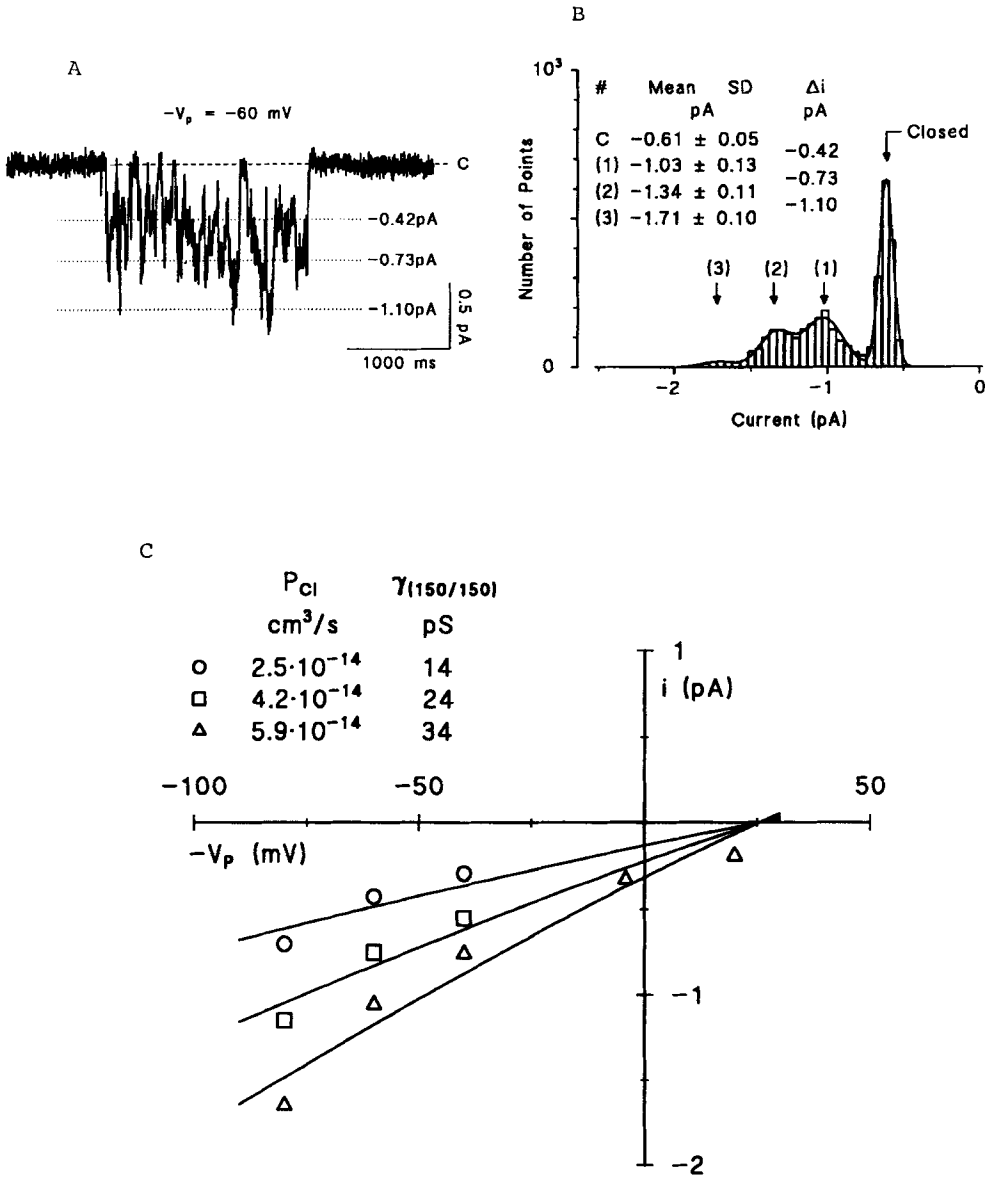

FIGURE 6. A cell-attached patch containing at least three apparently similar insect chloride channels. Bath $[Cl^-]$ = 150 mM, pipette $[Cl^-]$ = 40 mM. (*A*) Trace of a brief period of channel activity at $-V_P$ = −60 mV. Closed-level (*C*) and means of Gaussian fits (see Fig. 6 *B*) are indicated by horizontal dashed lines. (*B*) Histogram distribution of the digitized current segment shown in Fig. 6 *A*, with the fit of the sum of four Gaussian distributions indicated by the full line. Besides the closed state (*C*), three open states were identified, here denoted by *1*, *2*, and *3*, respectively, with their Gauss parameters listed in the inserted table. (*C*) By a similar type of analysis, three conductance levels were also resolved at $-V_P$ = −80 and −40 mV, shown here together with two more opening events resolved at $-V_P$ = −10 mV and +20 mV. It is indicated that they belong to three different *i/V* relationships with GHK permeabilities as follows: (○) $P_{Cl} = 2.5 \cdot 10^{-14}$ cm³/s; (□) $P_{Cl} = 4.2 \cdot 10^{-14}$ cm³/s; and (Δ) $P_{Cl} = 5.9 \cdot 10^{-14}$ cm³/s. With V_{LJ} = +8 mV (Table I), the other GHK parameters are $[Cl^-]_C$ = 71 mM, V_C = −19 mV. To obtain these estimates of P_{Cl}, the GHK fits to the data given by the symbols ○ and □ were forced through the reversal potential estimated by the *i/V* relationship indicated by △. R_{seal} = 72 GΩ.

21 out of 62 patches of β-Gal cells studied in cell-attached mode. All channels resolved showed complex activity. This applied to open-close kinetics as well as to single-channel conductance distributions and was independent of whether or not the cell was infected with recombinant baculovirus and expressing cloned β-galactosidase.

Single-channel permeabilities. The channel shown in Fig. 5 exhibited long open times, often lasting several seconds, and was very noisy in the open state. The current–voltage relationship of the channel indicated a reversal potential near the spontaneous membrane potential (i.e., zero pipette potential) and shallow outward rectification as expected for a Cl^- channel. The GHK permeability of $P_{Cl} = 4.0 \cdot 10^{-14}$ cm^3/s indicates that its physiological conductance is $\gamma_r = 17$ pS (Eq. 3b), and that the channel would have been resolved with a conductance of $\gamma_{150/150} = 23$ pS in an excised inside-out patch bathed in symmetrical 150-mM Cl^- (Eq. 3c).

In most cases, several conductance states were seen in the same patch. A typical example is given in Fig. 6, *A* and *B*, showing that within a single opening event,

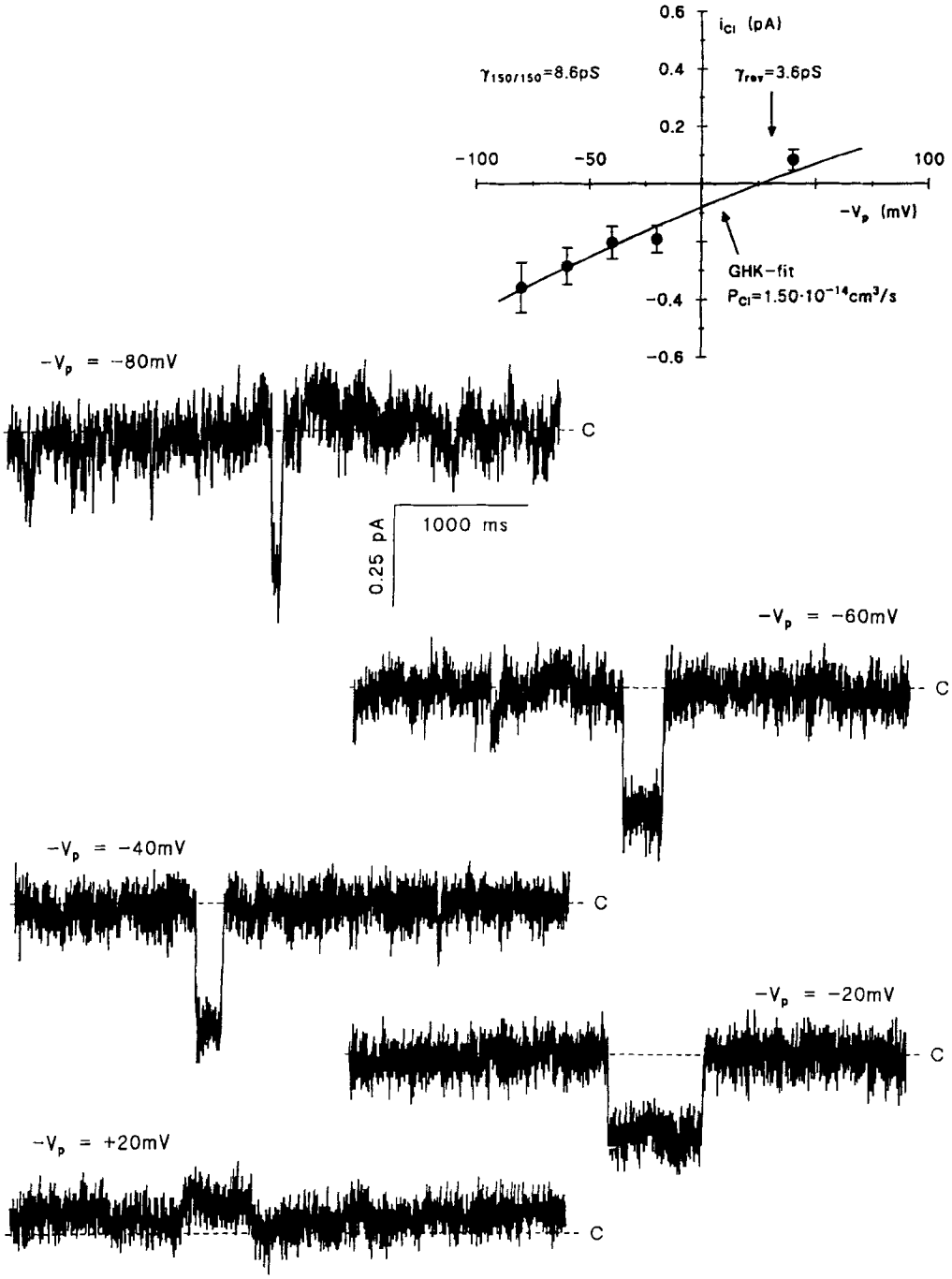

FIGURE 7. Cell-attached patch recordings of small endogenous chloride channel of *Sf*9 cell. Bath $[Cl^-]$ = 150 mM, pipette $[Cl^-]$ = 40 mM. (*A*) Shown are five current segments recorded at pipette potentials indicated above the traces and shown with similar gain and time scale. The *i/V* relationship was constructed from means of Gaussian fits to amplitude distribution histograms of digitized current, with SDs of the distributions indicated by vertical lines. The full line is the *i/V* relationship according to Eq. 2, with $P_{Cl} = 1.50 \cdot 10^{-14}$ cm^3/s, $[Cl^-]_C = 69$ mM, and $V_C = -19.6$ mV ($V_{LJ} = 8$ mV, Table I). $\gamma_{rev} = 3.6$ pS and $\gamma_{150/150} = 8.6$ pS were calculated by Eqs. 3b and 3c, respectively. $R_{seal} = 128$ GΩ.

the sampled currents could be resolved in four Gaussian distributions spaced $\sim\Delta i = -0.4$ pA from one another (Fig. 6 *B*). Similar results were obtained at other pipette potentials and, as revealed by the resulting *i/V* diagrams in Fig. 6 *C*, this patch seemed to contain three channels each of permeability, $P_{Cl} \cong 2 \cdot 10^{-14}$ cm^3/s. Fig. 7 shows another small channel. In this case, discrete steplike changes in current were resolved at several pipette potentials. The associated *i/V* relationship, measured in the physiological range of potentials, indicated a similar small conductance channel with permeability, $P_{Cl} \cong 1.6 \cdot 10^{-14}$ cm^3/s.

Another example of channels exhibiting simultaneous activity interrupted by long quiescent periods is given in Fig. 8. Here, four channels (*upper panel*) and six channels (*lower panel*) were simultaneously active. However, a single channel, with a noisy open state, also became active (*middle panel*). In this case, the limiting Cl^- channel conductance ($\gamma_{150/150}$) was no more than $\sim$4 pS. This was the smallest chloride channel resolved in cell-attached patches, and it was identified with certainty in eight patches ($\gamma_{150/150} = 3.7 \pm 0.5$, $n = 8$). Interestingly, a chloride channel of a similar conductance (<4 pS) was also observed in the first study using *Sf*9 cells expressing CFTR. Like in the present study, this small channel was characterized as an endogenous channel, and it was found in uninfected as well as in β-Gal–infected *Sf*9 cells (Kartner et al., 1991). In 21 cells, the largest identified level corresponded to $\gamma_{150/150} =$ 30–35 pS (see Fig. 6). Another frequently observed conductance level was similar to the previously noted 8–11-pS channel in a study of excised inside-out patches (Gabriel et al., 1992). In this former study, it was described as a "small linear channel" and observed in 60 out of 91 patches of uninfected *Sf*9 cells.

Single-Channel Recordings in Excised Patches

Excised inside-out patches. Endogenous channels in this configuration were first characterized in uninfected *Sf*9 cells (Gabriel et al., 1992), and few additional patches were generated in the present study. Presented here are recordings from β-Gal cells, confirming that with similar bath and pipette [Cl^-], the channel in excised inside-out configuration is linear. Fig. 9 shows a small 12-pS chloride channel resolved in an experiment where the major cation in bath and pipette was $Tris^+$. The long closed states interrupted by noisy open states, as well as jumps from the main state to sub- and superstates, resemble features of chloride channels resolved both in cell-attached (above) and in outside-out configurations (below).

Excised outside-out patches. With pipette resistance of 2–4 MΩ, we studied 26 patches excised from the whole-cell configuration. All 26 patches contained several active channels, which were not always easy to study. Simi-

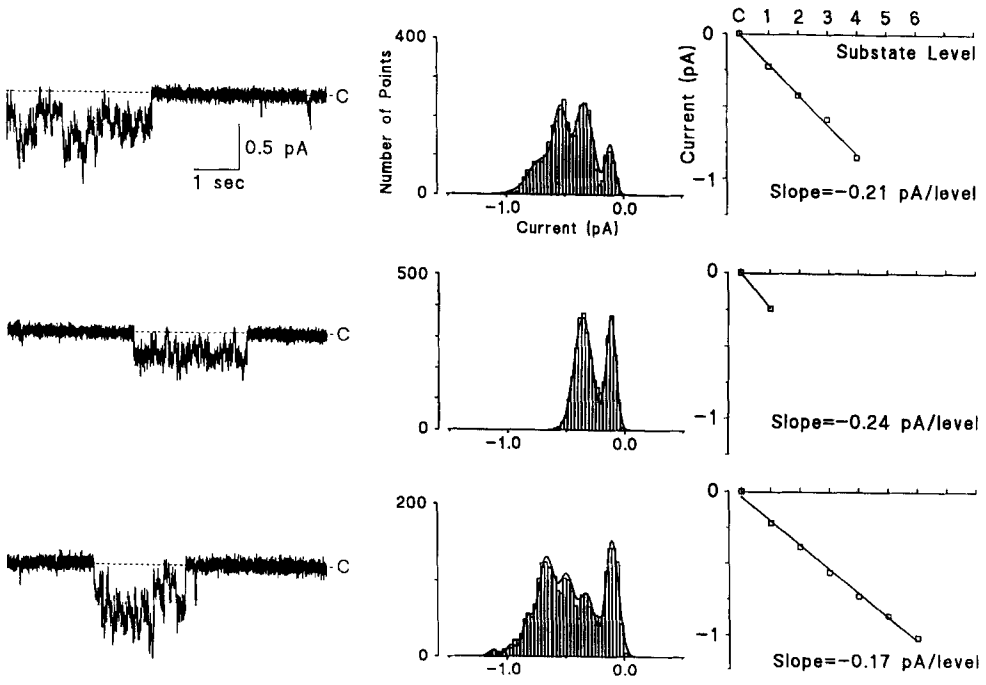

FIGURE 8. Cell-attached patch recordings showing several conductance levels associated with insect chloride channel activity. Bath [Cl^-] = 150 mM, pipette [Cl^-] = 40 mM, $-V_P = -40$ mV. (*Left*) Three different current segments from the same patch recording, but with different types of activity. In the upper trace, sampling of the analog signal started within an activity period. (*Middle*) Histograms of digitized current distributions of the traces shown in the left column with sum of fits of Gaussian distributions shown as full lines. (*Right*) Relationships between conductance levels, identified by histogram distributions, and mean current of Gaussian fits. The slopes of linear regression analyses indicate that the patch contained at least six small channels of similar conductance. $R_{seal} = 191$ GΩ.

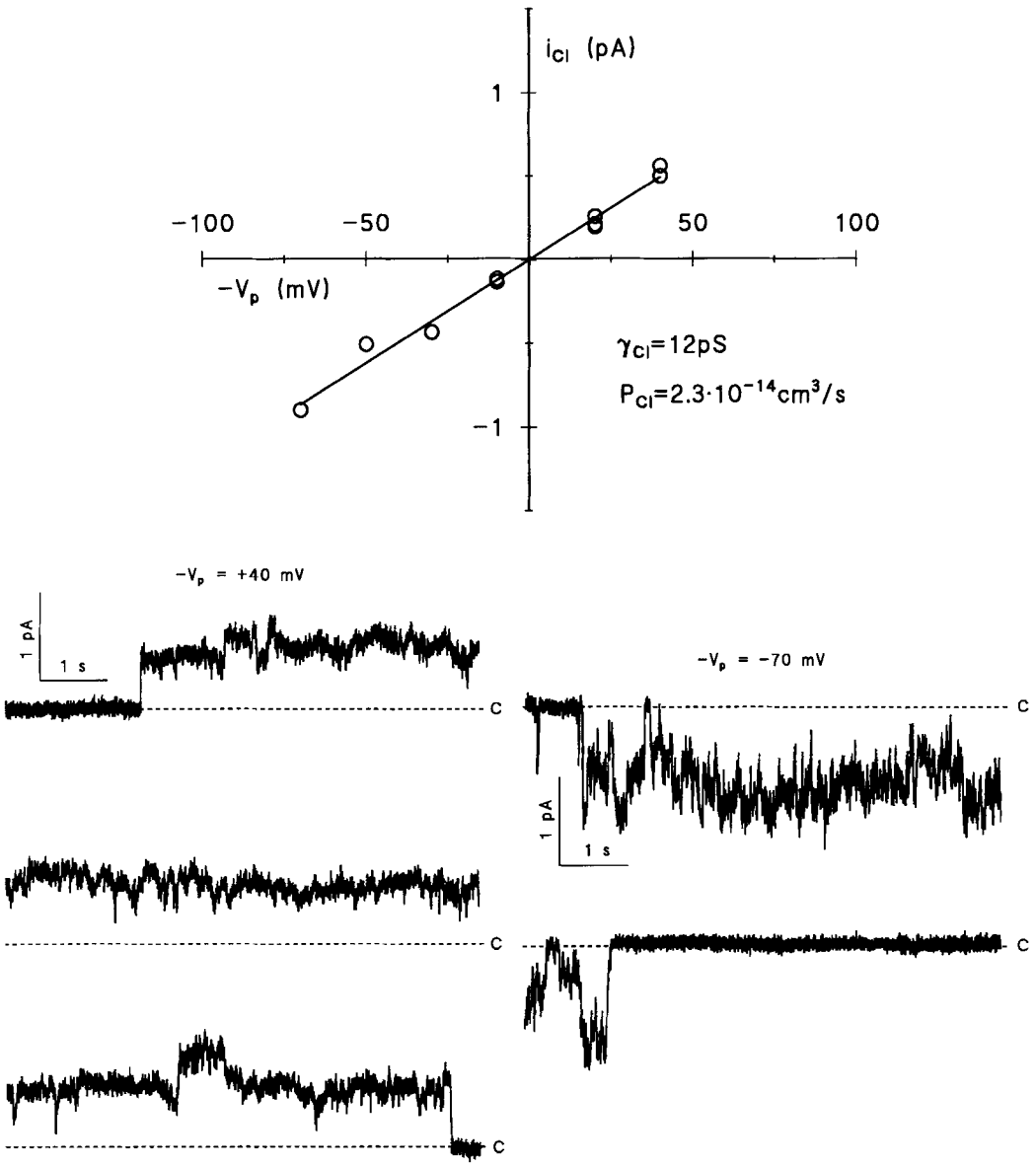

FIGURE 9. Small linear chloride channel of excised inside-out patch. Bath [Cl^-] and pipette [Cl^-] = 150 mM with $Tris^+$ as major cation. The traces shown in the lower left ($-V_P$ = +40 mV) are from a continuous recording of an ~20-s-long opening. Similar long openings were observed at all potentials studied, and one other is shown by the traces in the lower right (~10 s, $-V_P$ = −70 mV). The *i/V* relationship was obtained from Gaussian fits to all-point distributions of the main conductance states (defined by long dwell-times).

lar to cell-attached patches, the electrical activity of individual outside-out patches revealed conductance levels spanning a considerable range of amplitudes as well as noisy openings lasting several seconds. Because of heterogeneity among event amplitudes, it was not always possible to obtain the channel's *i/V* relationship.

The recordings shown in Fig. 10 were all obtained in the same patch and at a pipette potential of V_p = 50 mV. Because of the low extraneous noise level, event amplitudes (Δi) as small as 0.10–0.20 pA were easily resolved (Fig. 10, *A* and *E*). Events of other well-defined amplitudes were also resolved, of which the largest one was $\Delta i \cong$ 1.2 pA (Fig. 10, *C* and *G*). A frequently observed event amplitude was $\Delta i \cong$ 0.8–0.9 pA (Fig. 10 *D*), and histogram analysis of digitized points of this current segment revealed the simultaneous activity of two such channels (Fig. 10 *H, bottom row*). The closure of an event of ~0.35 pA, i.e., about twice the smallest resolved amplitude, is seen in Fig. 10 *B*. In this case, activity was initiated by an opening with a current amplitude of ~0.61 pA, i.e., about four times the smallest resolved amplitude, from which the current then jumped to Δi = 0.35 pA. An opening with similar amplitude (Δi = 0.37 pA; Fig. 10 *F*) made a transition to Δi = 1.24 pA before full closure. The event amplitudes resolved in this patch at pipette potential, V_p = 50 mV, depicted a straight-line relationship (r^2 = 0.991) with a slope of 0.14 pA/state (see Fig. 12 *A*). These observations suggest that the patched membrane contained at least eight small channels, each of which carries a current of ~140 fA in its open state.

To ascertain whether small as well as large amplitude

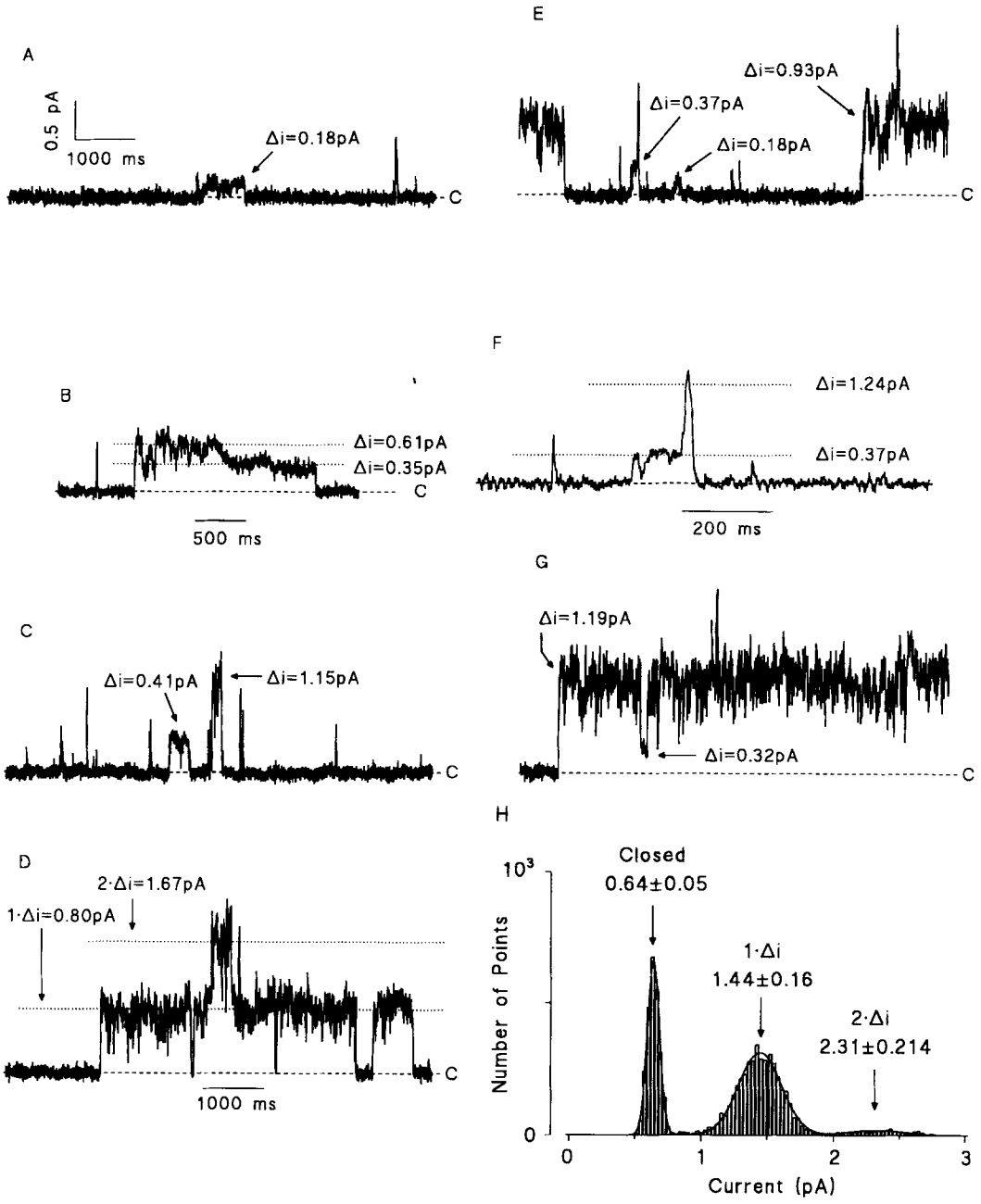

FIGURE 10. Excised outside-out patch exhibiting multiple conductance levels. Bath $[Cl^-]$ = 150 mM, pipette $[Cl^-]$ = 40 mM. Driving force clamped at V_P = 50 mV. The common gain for all traces is indicated in the upper left. Unless otherwise indicated, the time scale is as shown in the upper left. Conductance levels are given as current amplitudes from closed state obtained by histogram analysis of current distributions as exemplified in the lower left and right. R_{seal} = 41 GΩ.

transitions were all associated with a flow of chloride ions, the patch was studied at other pipette potentials. As seen in Fig. 11, within the range of the much smaller physiological driving forces (V_p = 0 mV and −60 mV), more than one type of amplitude transition was observed. When individual current amplitudes are depicted against pipette holding potential, a common reversal potential near the estimated chloride equilibrium potential was clearly identified, with GHK permeabilities spanning the range from $0.6 \cdot 10^{-14}$ to $5.6 \cdot 10^{-14}$ cm³/s (see Fig. 12 *B*). With a reversal potential of V_{rev} = −25 mV, the slope of the linear relationship obtained in Fig. 12 *A* (140 fA/state) corresponds to a unitary channel conductance of no more than 1.9 pS, or a limiting conductance of $\gamma_{150/150}$ = 3.4 pS (Fig. 12 *B*), which is of a magnitude similar to the smallest channel resolved in cell-attached patches.

In outside-out patches, openings of very long durations were also encountered. Once a channel entered a kinetic state of very long openings, another one or two similar channels might be observed. In the example shown in Fig. 13 *A*, the patch contained at least three similar channels. Note here that once the first channel opened, it stayed open for ~30 s, then two more channels became active. These long openings, interrupted by similar long periods of no activity at all, allowed the

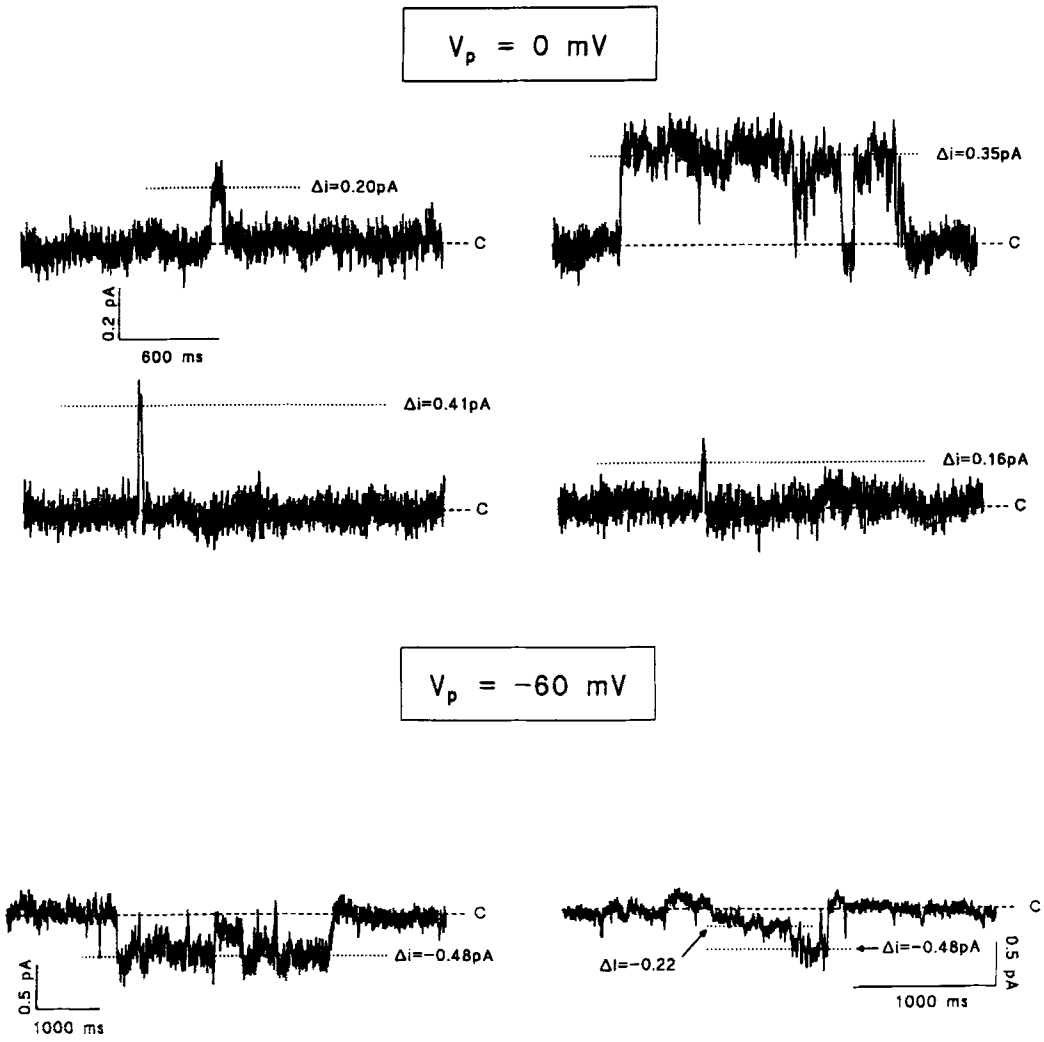

FIGURE 11. Outside-out patch exhibiting multiple conductance levels. Same patch as shown in Fig. 10, here for V_P = 0 and −60 mV.

construction of the channel's *i/V* relationship. This measurement was done by imposing a series of voltage pulses across the patch, while the channel was open (i_{total}) and closed (i_{seal}). The open-channel *i/V* relationship (Fig. 13 *B*) indicates a GHK permeability of ~2.6 · 10^{-14} cm^3/s, corresponding to a limiting conductance ($\gamma_{150/150}$) of ~15 pS. Often, outside-out patches entered into such periods of activity with open and closed states of very long durations (in the order of 30 s). The number of events sampled during these (unpredictable) periods of activity was too small for analyzing open- and closed-time distributions.

Kinetics of Single-Chloride Channel Activity

Generally, all channels resolved exhibited slow as well as fast gating, which are well documented by recordings shown above. Thus, inspection of the activity of both cell-attached patches (e.g., Fig. 5) and excised patches (e.g., Figs. 10 and 13 *A*) reveals fast gating within openings interrupted by long quiescent periods. We could not, however, follow up this observation with a quantitative analysis of open and closed dwell-time distributions. This was due to the fact that the patches exhibited conductance transitions indicating more than a single open state. Another way to analyze single-channel kinetics would be to generate the PDS of the current fluctuations caused by channel activity in patched membranes. Such spectra are shown in Fig. 14. Clamping the pipette potential to a value where the chloride ion distribution is at equilibrium (V_p = 0 mV; Fig. 14 *A*) resulted in a very significant reduction of the power at all frequencies. This shows that the PDS over a wide range of frequencies is governed by the activity of and current flow in chloride channels. Furthermore, independent of patch configuration, i.e., cell-attached patches (Fig. 14 *A*) or excised outside-out patches (Fig. 14 *B*), the PDS of single-channel transitions contained more than one Lorentzian component. The lowest corner frequency (f_{c1} = 0.40 ± 0.02 Hz, n = 4) corresponds to that obtained by our analysis of whole-cell current fluctuations (Table III). The close similarity of

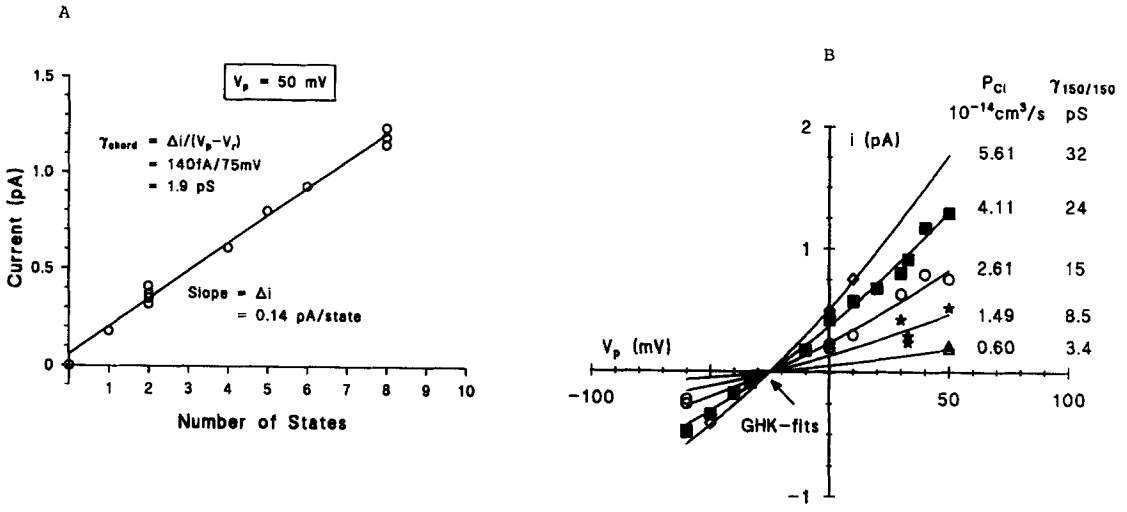

FIGURE 12. Endogenous insect chloride channels of *Sf*9 cells. Analysis of multiple conductance levels of excised outside-out patch. Same patch as in Figs. 10 and 11. (*A*) The conductance levels resolved at V_P = 50 mV depicted a linear relationship with a unitary current amplitude Δi_{unit} = 140 fA. With a reversal potential V_P = −25 mV (Fig. 12 *B*), the unitary chord conductance would be γ_{chord} = 1.9 pS. (*B*) Current–voltage curves of five of the resolved conductance levels of the patch. (*Inset*) Permeability coefficients of the GHK fits are indicated by full lines. Limiting conductances were calculated according to Eq. 3c.

the PDS of identified single-Cl^- channel transitions (Fig. 14, *A* and *B*) and that of whole-cell current fluctuations (Figs. 1, 3, and 4) leads to the conclusion that the macroscopic PDS is governed by the activity of chloride channels. Thus, in an independent way, the spectra shown in Fig. 14 confirm the conclusion drawn from the data shown, for example, in Figs. 1, 3, and 4 and compiled in Table III, that a very significant fraction of

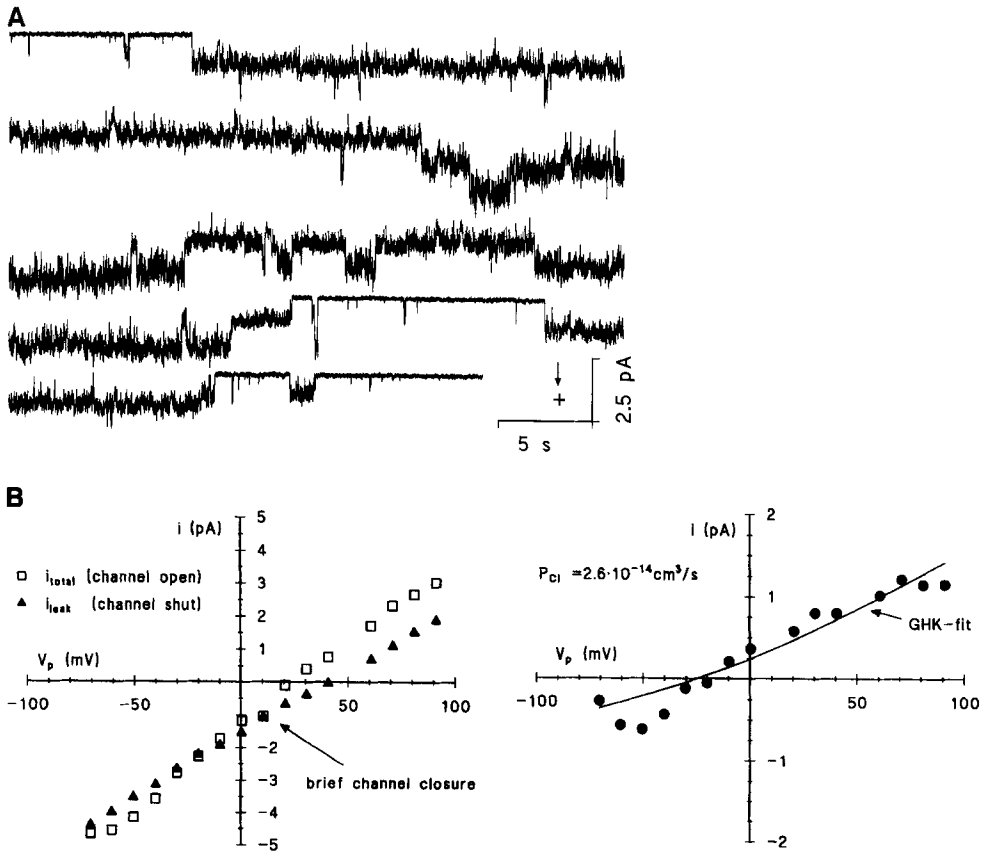

FIGURE 13. Locked open state of insect chloride channel in excised outside-out patch of *Sf*9 cell. Bath [Cl^-] = 150 mM, pipette [Cl^-] = 40 mM, V_P = 50 mV. (*A*) Beginning in the upper left, 155 s of continuous recording with positive open-channel currents going downward is shown. (*B, left*) Current responses to pulsing V_P, held at +50 mV, in steps incremented by ±10 mV and of 200-ms duration covering the range of −70 to +90 mV. i_{total}, currents generated while a single channel, shown in Fig. 13 *A*, was open (however, at V_P = 10 mV, the channel entered a closed state); i_{leak}, currents generated while the patch was silent. (*B, right*) Resulting current–voltage relationship of single insect chloride channel obtained by subtraction, $i = i_{total} - i_{leak}$. Fitting of Eq. 2 provided an estimate of single-channel permeability, $P_{Cl} \approx 2.6 \cdot 10^{-14}$ cm^3/s, and a limiting conductance ($\gamma_{150/150}$) of ~15 pS. R_{seal} = 26 GΩ.

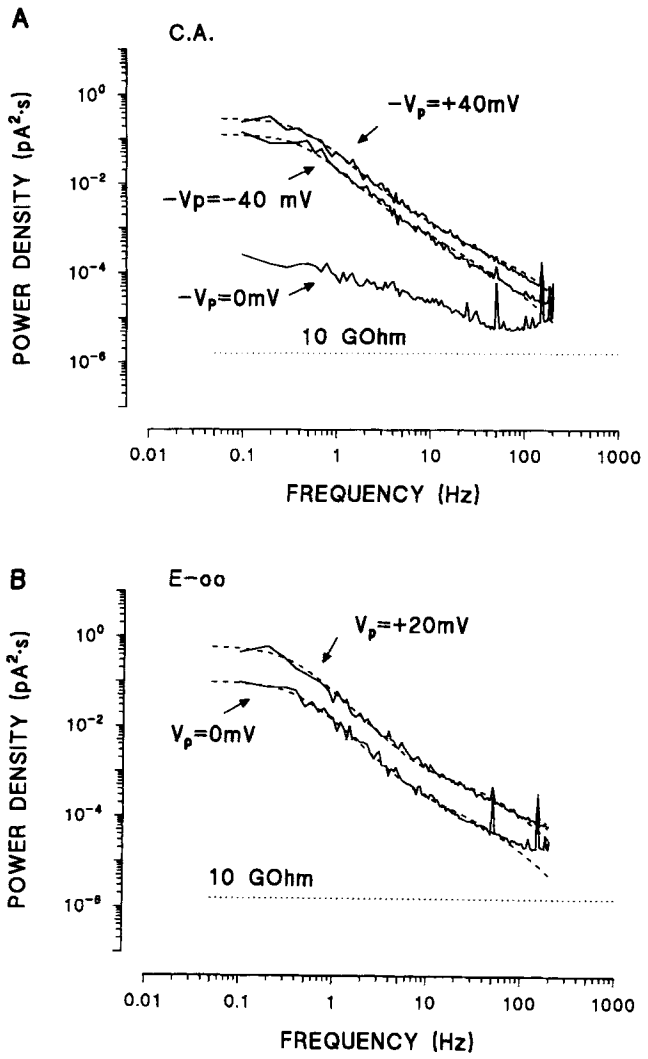

FIGURE 14. PDS of Cl^- current flow in membrane patches of *Sf*9 cells. Blocksize 4096, bandwidth 200 Hz (−3 dB, eight-pole Butterworth). (*A*) Cell-attached patch with identical (standard) solutions in pipette and bath (Materials and Methods), and pipette potential clamped at the three different values indicated. The three spectra shown are from the same patch. Dashed lines are calculated as the sum of three Lorentzian components (Eq. 6b) with the following parameters. $-V_p$ = +40 mV: f_{c1} = 0.42 Hz, S_{01} = 0.30 pA² · s; f_{c2} = 9.25 Hz, S_{02} = 1.3 · 10^{-3} pA² · s; f_{c3} = 85.6 Hz, S_{03} = 2 · 10^{-4} pA² · s $-V_p$ = −40 mV: f_{c1} = 0.43 Hz, S_{01} = 0.13 pA² · s; f_{c2} = 11.3 Hz, S_{02} = 6.2 · 10^{-4} pA² · s; f_{c3} = 56 Hz, S_{01} = 8 · 10^{-5} pA² · s. Here, and in *B*, the high frequency powers were omitted for obtaining the Lorentzian fits to the calculated spectra.The PDS obtained at V_p = 0 mV (V_m = E_{Cl}) indicates the noise floor of the recording setup which is not "white" and somewhat larger than the theoretical minimum level given by the Johnson-Nyquist noise of the headstage's feedback resister (10 GΩ; Eq. 6a). The line frequency here is 50 Hz (University of Copenhagen) compared with 60 Hz in Fig. 3 (University of North Carolina at Chapel Hill). (*B*) Excised outside-out patch with standard bath ([Cl^-] = 150 mM) and pipette ([Cl^-] = 40 mM) solutions (Materials and Methods). The two spectra were obtained from the same patch. The Lorentzian parameters used for construction of the dashed relationships are V_p = +20 mV: f_{c1} = 0.33 Hz, S_{01} = 0.61 pA² · s; f_{c2} = 40 Hz, S_{02} = 5 · 10^{-4} pA² · s; f_{c3} = 75 Hz, S_{03} = 1 · 10^{-4} pA² · s. V_p = 0 mV: f_{c1} = 0.40 Hz, S_{01} = 0.10 pA² · s; f_{c2} = 27 Hz, S_{02} = 1.3 · 10^{-4} pA² · s; f_{c3} = 79 Hz, S_{01} = 2 · 10^{-5} pA² · s.

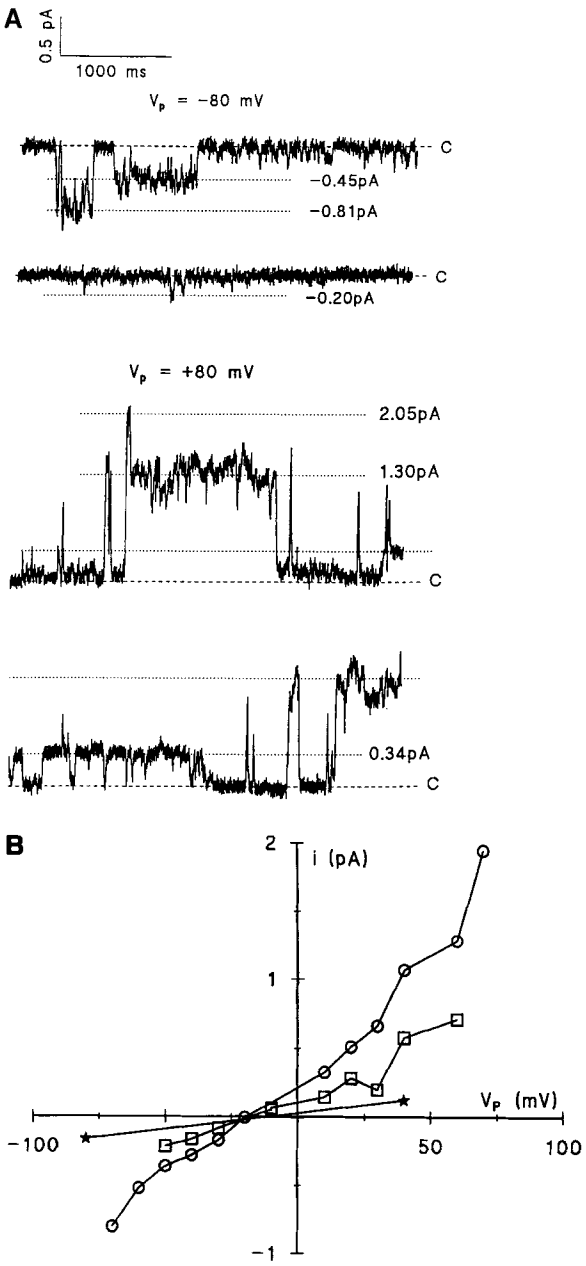

FIGURE 15. Analysis of Br^-/Cl^- selectivity of conductance levels resolved in excised outside-out patch of insect *Sf*9 cell. $[Br^-]_B$ = 100 mM; $[Cl^-]_B$ = 50 mM; $[Br^-]_P$ = 10 mM; $[Cl^-]_P$ = 40 mM. (*A*) Currents obtained at pipette potentials of −80 mV (*two upper traces*) and +80 mV (*two lower traces*). Conductance levels are indicated by current jumps from closed state resolved by Guassian fits to histograms of current distributions. (*B*) Currrent–voltage relationships of three resolved conductance levels indicate a common reversal potential.

the variance of the whole-cell membrane current fluctuations is governed by slowly gated chloride channels.

Halide Ion Selectivity of Individual Conductance States

It was shown above that it was possible, in the same patch, to retrieve information on a set of channel events at different membrane potentials for the construction of families of *i/V* relationships (Figs. 6 and 13). However, after a change in external halide ion composition, it was no longer possible to associate the individual conductance levels with those identified before the change of solution. Therefore, with such a protocol we could not analyze shifts in reversal potentials to obtain information on the selectivity of the conductance levels. It turned out, however, that families of *i/V* curves could be obtained in experiments where chloride ions were partly replaced by either bromide or iodide. With this protocol, we needed just a single set of *i/V* relationships for calculating channel selectivities. As can be seen by the recordings shown in Fig. 15 *A*, with both Br^- and Cl^- in bath and pipette solution, several different channel amplitudes were observed in the same patch. Three channels were resolved, and they were all found to reverse near −20 mV (Fig. 15 *B*). After correction for a liquid junction potential of 6.3 mV (Table I; Eq. 1b) the reversal potential entering Eq. 4 is $V_{rev} \cong -26.3$ mV, from which we calculate a selectivity ratio of $P_{Br}/P_{Cl} \cong 0.90$ ($P_{Br}/P_{Cl} = 0.93 \pm 0.08$, $n = 3$; the ratio is not statistically different from unity).

Also, in patches studied with a Cl^-/I^- ion pair, several different event amplitudes were resolved. Fig. 16 shows current segments obtained with pipette potential held at +50 mV, i.e., with a large inwardly directed driving force imposed on the halide ions. Despite clamping the driving force to a constant value, the current jumped to several levels, apparently in a random fashion. The largest event was ~1.8 pA, but several other open states of long dwell-times are also seen. Similar sets of observations were obtained at other membrane potentials. From inspection of the current records shown in Fig. 17, it can be seen that currents all reversed at a pipette potential near −30 mV. The family of *i/V* relationships constructed from these current records is shown in Fig. 18 *A*. Individual current–voltage curves were near-linear, with slopes ranging from 3.7 to 22.1 pS. Fig. 18 *B* shows that individual conductance levels were a multiple of the smallest conductance resolved ($r^2 = 0.993$). On the average, with this ion pair a reversal potential of 30.0 ± 2.7 mV ($n = 8$) was obtained. With $V_{LJ} = +5.8$ mV (Table I), the estimate of the reversal potential of all conductance levels is $V_r \approx -35.8$ mV. From this value we calculate a selectivity ratio of $P_I/P_{Cl} = 2.0$.

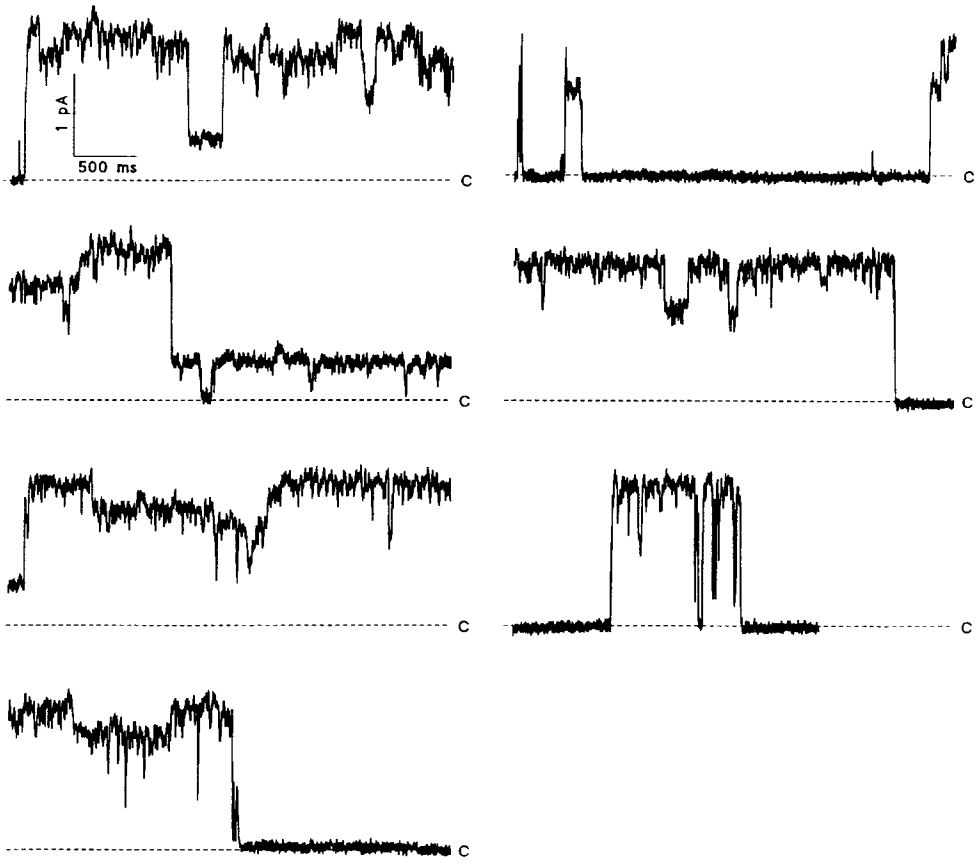

FIGURE 16. Analysis of I^-/Cl^- selectivity of conductance levels resolved in excised outside-out patch of insect *Sf*9 cell. $[I^-]_B = 100$ mM; $[Cl^-]_B = 50$ mM; $[I^-]_P = 10$ mM; $[Cl^-]_P = 40$ mM. At a constant $V_P = 50$ mV, current jumps to several different levels are seen. $R_{seal} = 91$ GΩ.

DISCUSSION

This study has shown that fluctuations of whole-cell chloride currents in insect *Sf*9 cells cannot simply be the result of random opening and closing of just a single population of two-state ionic channels. It has further been demonstrated that membrane patches of these cells contain channels of multiple time constants and multiple conductance levels. Here, we shall discuss causal relationships between the gating features revealed in whole-cell and in single-channel recordings, respectively. The other question to be addressed is whether different levels of single-channel conductance result from simultaneous opening and closing of a varying number of smaller but similar channels.

Fluctuations of Whole-Cell Currents Reveal Multiple Gating Modes of Chloride Channels

Whole-cell recordings showed that the major membrane current was carried by channels specific for Cl^- (Fig. 2, Table II). In this situation and with a well-defined high frequency background noise, it was fairly easy to verify that fluctuations of membrane currents recorded in the band, Δf = 2–1,000 Hz, were caused by chloride channel activity (Fig. 3, *A* and *B*). However, the membrane currents also displayed low frequency fluctuations, and they contributed relatively significantly to the total variance at all potentials (Table III). Therefore, although some spectra became fairly flat below 1 Hz, it is important to consider to what extent extraneous noise contributed to the low frequency power. To deal with this question in detail, we analyzed the relative contributions of different background noise sources to the variance of current fluctuations in the entire frequency range of interest. At higher frequencies, the spectra generated by nonbiological sources were well predicted by theoretical considerations. For $f < 2$ Hz, the background spectrum deviated from theory by rising rather steeply with decreasing frequency, however, with unpredictable "roll-off" (cf. Figs. 1 and 3). With 970-pA DC current flowing to ground, the PDS of the nonbiological noise source was several orders of magnitude smaller than that of whole-cell currents of similar magnitude (Fig. 1). Thus, it is indicated that, also at the lowest frequencies, the PDS of *Sf*9 membrane currents is produced by electrical activity of ion channels.

Single-channel recordings supported this contention. Chloride channels studied both in cell-attached (Fig. 5), in excised inside-out (Fig. 9), and in excised outside-out patches (Figs. 11, 15 *A*, 16, and 17) entered into open states of 0.1–5-s durations interrupted by similar long closed states. The channels also exhibited faster gating modes, seen as brief closures within the long periods of openings. Furthermore, the resulting PDS, whether calculated from current flow in cell-attached (Fig. 14 *A*) or excised outside-out (Fig. 14 *B*) patches, shows sufficient similarity with that of the whole-cell current fluctuations to allow the conclusion that whole-cell currents and their fluctuations about their stationary mean value—over the entire frequency range covered in this study—are generated by the electrical activity of chloride channels.

This said, it is equally important to note that the very long open states exemplified in Fig. 13 *A* might well contribute to additional power below the frequency range we are able to study. The lower frequency limit for spectral analysis of whole-cell current fluctuations is defined by the slowly developing undesired current drift (e.g., Conti et al., 1980; Helman and Kizer, 1990). An investigation of the possible contribution of the very slow gating to the macroscopic PDS would require sampling of currents for 20 min or more. We could not acquire stationary whole-cell currents for such a long period of time.

Multiple Conductance States Indicate the Presence of Elementary Channel Units

Identification of channel currents. In cell-attached patches, endogenous K^+ channels of *Sf*9 cells reverse at pipette potentials between 85 and 100 mV and carry outward currents when V_P is held at 0 mV (Claus Nielsen and E. Hviid Larsen, unpublished observations). Thus, K^+ currents are easily distinguished from Cl^- currents which, with $[Cl^-]_P = [Cl^-]_B$, reversed near $V_P = 0$ mV (Fig. 5). In agreement with this notion, when $[Cl^-]_P$ was lowered significantly, i.e., from 150 to 40 mM, currents carried by cell-attached channels reversed at $-V_P > 0$ mV (Fig. 7). In excised outside-out patches with $Tris^+$ as major cation in pipette solution, cation (Na^+) channel currents would reverse at $\sim$+60 mV. However, all channel currents resolved in this configuration reversed near the major anion's negative reversal potential (e.g., Fig. 13 *B*). Thus, it was not difficult to identify the conducting ion in electrically active channels. In the present study, we never observed membrane patches with cation-selective channels. With this information and results of the whole-cell current analysis (Fig. 2 and Table II), it seems that *Sf*9 cells grown under the present conditions express a relatively very low cation permeability. Since they also generate a fairly small membrane potential, $V_C \cong -15$ mV,[2] cultured *Sf*9 cells share macroscopic membrane electrophysiology with mammalian red cells. They exhibit a small membrane potential, a relatively very low cation permeability, and

[2]Similar to all whole-cell and single-channel current recordings, the membrane potential was measured in cells bathed in a solution made slightly hypertonic by 50 mM sucrose; see Materials and Methods.

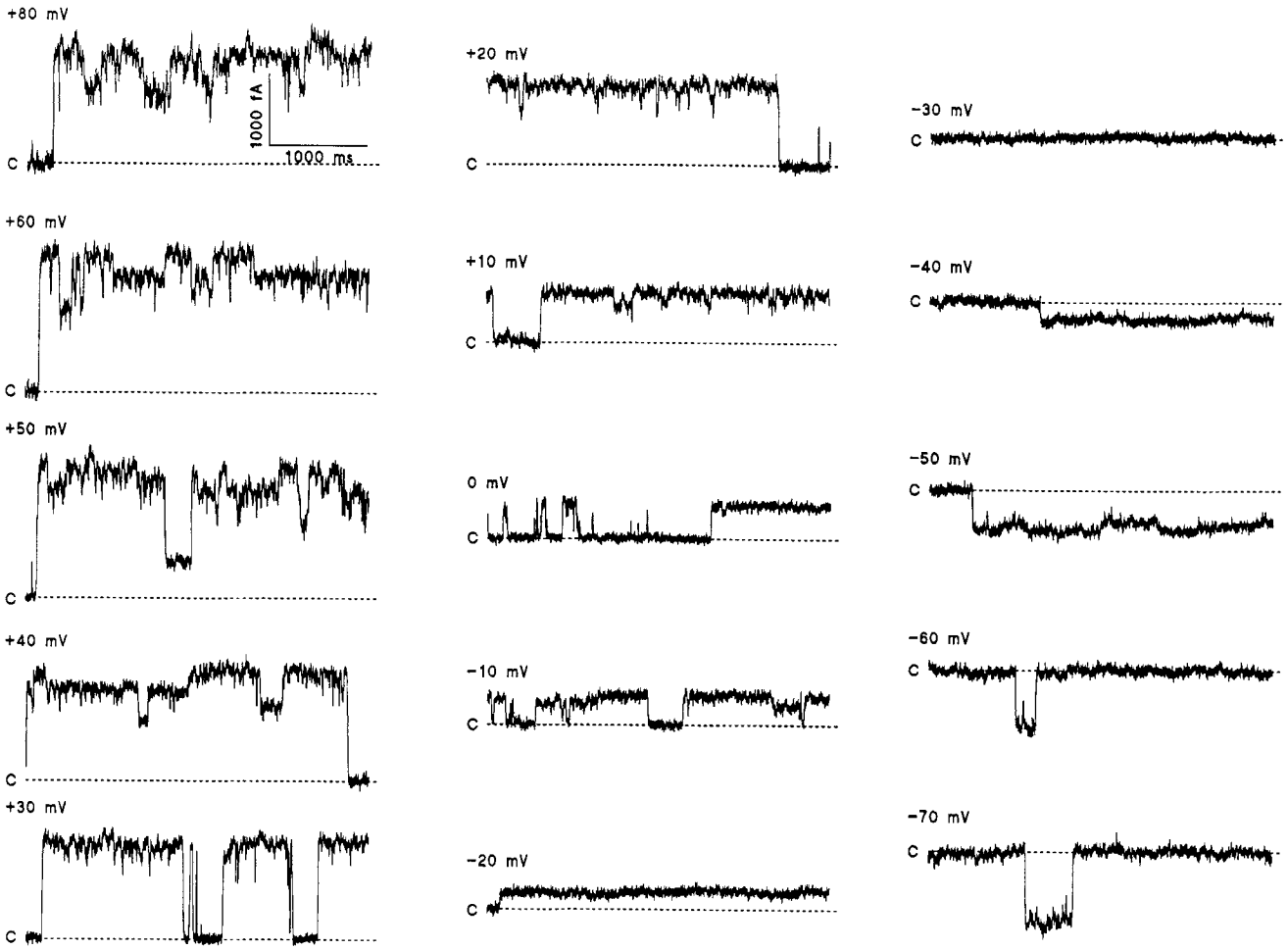

FIGURE 17. Analysis of I^-/Cl^- selectivity of conductance levels resolved in the excised outside-out patch of Fig. 16. Current recordings at 15 pipette potentials covering the range from +80 to −70 mV with V_P indicated above each trace (the trace shown for V_P = +50 mV is the same as the one in Fig. 16, *upper-left*. $[I^-]_B$ = 100 mM; $[Cl^-]_B$ = 50 mM; $[I^-]_P$ = 10 mM; $[Cl^-]_P$ = 40 mM.

an intracellular chloride concentration of ~75 mM (Bennekou and Stampe, 1988; Parker and Dunham, 1989).

Rectification and permeability. Independent of membrane patch configuration, open-channel currents were well described by the GHK equation both for inward and outward currents. In agreement with this notion, rectification switched from outward (Figs. 5 and 13) to inward when external $[Cl^-]$ was made significantly lower than the estimated internal $[Cl^-]$ (Fig. 7). Like the macroscopic membrane currents (Fig. 2), the *i/V* relationship became linear, as predicted, for symmetrical Cl^- concentrations (Fig. 9). A useful conse-

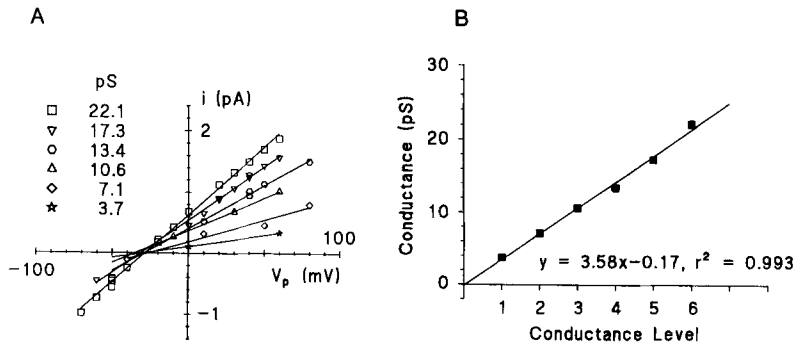

FIGURE 18. Analysis of I^-/Cl^- selectivity of conductance levels resolved in the excised outside-out patch of Figs. 16 and 17. (*A*) The patch exhibited at least six different conductance levels. The associated current–voltage relationships were near-linear with a common reversal potential far more left than that obtained with Br^-/Cl^- as halide ion pair (Fig. 15 *B*), indicating a strong preference for iodide over chloride and bromide. (*Inset*) Slope conductances obtained by linear regression analyses. (*B*) The slopes of individual current–voltage relationships depicted a straight line as a function of conductance level with unitary conductance γ_{slope} = 3.6 pS.

quence of this consistent ion permeation mode is that one can calculate an intrinsic conductance property, such as permeability or limiting conductance ($\gamma_{150/150}$), to compare channels resolved in different configurations, bathing solutions, or range of potentials. Chloride channels resolved in cell-attached as well as in excised patches exhibited several conductance levels (e.g., Figs. 6, 8, 10, 11, 16, and 17), indicating a hallmark of the endogenous chloride ion permeation system in *Sf*9 cells. Thus, permeabilities obtained from single-channel *i/V* curves ranged from $\sim 0.5 \cdot 10^{-14}$ cm^3/s to $\sim 5.5 \cdot 10^{-14}$ cm^3/s in cell-attached patches as well as in excised outside-out patches with the associated limiting conductance levels spanning from 3–4 pS to ~35 pS.

Interrelationship between conductance levels. With the driving force for current flow held constant, currents exhibited transitions of different amplitudes with large as well as smaller current transitions occurring from, and to, the closed level, as well as from one open level to another (Figs. 10, 16, and 17). Different conductance levels reversed near the same potential (Figs. 6 and 12) and exhibited a halide ion permeation sequence of $P_I > P_{Cl} \cong P_{Br} = 2.0{:}1{:}0.9$ (Figs. 15 and 18 *A*). In other words, the selectivity is common for all conductance levels studied. Furthermore, the smallest conductance resolved was similar in cell-attached and excised outside-out patches, i.e., $\gamma_{150/150} = \sim 3.5$ pS. These observations lead to the question of whether different conductance levels are associated with jumps from a main conductance state to substates and superstates of a single-channel molecule or are caused by simultaneous activity of several channel molecules. If a jump from one conductance level to another is associated with a transition of a single-channel molecule, one would have to postulate six or more states of the conducting pore (Figs. 12 and 18), with every state separated from its two neighboring states by exactly the same distance (Fig. 18 *B*). Thus, because individual current amplitudes, independent of absolute value, could be resolved into an integer number of an elementary channel unit, it is more likely that several channel molecules contributed to the Cl^- current flow, with the number of electrically active channels varying from patch to patch and moment to moment. The number of active units could be quite large; e.g., six levels were resolved in Figs. 8 and 18, and 10 levels were calculated from the permeability coefficient of the largest channel studied (Fig. 12).

Mazzanti et al. (1991) proposed a model accounting for Ca^{2+} current–dependent block of L-type Ca^{2+} channels that assumed that calcium channels occur in clusters sharing a submembrane Ca^{2+} pool buildup by inflowing Ca^{2+} (see also DeFelice, 1993). Cell surface transport studies of murine glycoproteins (Holifield and Jacobson, 1991), of the low density lipoprotein receptor (Ghosh and Webb, 1993), of epidermal growth factor receptor and E-cadherin (Kusumi et al. 1993), and of the receptors for transferrin and α_2-macroglobulin (Sako and Kusumi, 1994) have indicated that these integral plasma membrane proteins are also confined to small membrane domains, e.g., governed by interactions with the cytoskeletal network adjacent to the membrane (Kusumi et al., 1993), rather than having a random horizontal distribution on the surface of the membrane. The results obtained in the present study with insect cells in culture indicate that (*a*) the plasma membrane chloride conductance consists of elementary chloride channel units, and that (*b*) single events of amplitudes larger than the elementary current flow result from coordinated open/close transitions of two or more elementary channel units. The finding that the number of units exhibiting simultaneous open/close activity varies from patch to patch, and from moment to moment in the same patch, would be consistent with the occurrence of channel units in membrane domains allowing for coordinated activity among two or more channel units.

This work was supported by National Institutes of Health grants HL34322 and P30DK34987 and by Danish National Science Research Council grants 110017, 119270, and 110971.

Original version received 27 June 1995 and accepted version received 27 February 1996.

REFERENCES

Anderson, C.R., and C.F. Stevens. 1973. Voltage clamp analysis of acetylcholine-produced end-plate current fluctuations at frog neuromuscular junction. *J. Physiol. (Camb.).* 236:655–691.

Bear, C.E., C. Li, N. Kartner, R.J. Bridges, T.J. Jensen, M. Ramjoesingh, and J.R. Riordan. 1992. Purification and functional reconstitution of the cystic fibrosis transmembrane conductance regulator (CFTR). *Cell.* 68:809–818.

Bennekou, P., and P. Stampe. 1988. The effect of ATP, intracellular calcium and the anion exchange inhibitor DIDS on conductive anion fluxes across the human red cell membrane. *Biochim. Biophys. Acta.* 1030:183–187.

Birnir, B., M.L. Tierney, S.M. Howitt, G.B. Cox, and P.W. Gage. 1992. A combination of human α1 and β1 subunits is required for formation of detectable GABA-activated chloride channels in

Sf9 cells. *Proc. R. Soc. Lond. Ser. B Biol. Sci.* 250:307–312.

Christensen, O., and N. Bindslev. 1982. Fluctuation analysis of short-circuit current in a warm-blooded sodium-retaining epithelium: site, current, density, and interaction with triamterene. *J. Memb. Biol.* 65:19–30.

Colquhoun, D., and A.G. Hawkes. 1977. Relaxation and fluctuations of membrane currents that flow through drug-operated ion channels. *Proc. R. Soc. Lond. Ser. B Biol. Sci.* 199:231–262.

Conti, F., B. Neumcke, W. Nonner, and R. Stämpfli. 1980. Conductance fluctuations from the inactivation process of sodium channels in myelinated nerve fibres. *J. Physiol. (Camb.).* 308:217–239.

DeFelice, L.J. 1981. Introduction to Membrane Noise. Plenum Press, New York and London. 500 pp.

DeFelice, L.J. 1993. Molecular and biophysical view of the Ca channel: a hypothesis regarding oligomeric structure, channel clustering, and macroscopic current. *J. Membr. Biol.* 133:191–202.

Finkelstein, A., and A. Mauro. 1963. Equivalent circuits as related to ionic systems. *Biophys. J.* 3:215–237.

Fisher, H., and T.E. Machen. 1994. CFTR displays voltage dependence and two gating modes during stimulation. *J. Gen. Physiol.* 104:541–566.

Fishman, H.M. 1973. Relaxation spectra of potassium channel noise from squid axon membranes. *Proc. Nat. Acad. Sci. USA.* 70: 876–879.

Gabriel, S.E., E.M. Price, R.C. Boucher, and M.J. Stutts. 1992. Small linear chloride channels are endogenous to nonepithelial cells. *Am. J. of Physiol. (Cell Physiol.).* 263:C708–C713.

Gadsby, D.C., G. Nagel, and T.-C. Hwang. 1995. The CFTR chloride channel of mammalian heart. *Annu. Rev. Physiol.* 57:387–416.

Ghosh, R.N., and W.W. Webb. 1993. Automated detection and tracking of individual and clustered cell surface low density lipoprotein receptor molecules. *Biophys. J.* 66:1301–1318.

Goldman, D.E. 1944. Potential, impedance, and rectification in membranes. *J. Gen. Physiol.* 27:37–60.

Hamill, O.P., A. Marty, E. Neher, B. Sakmann, and F.J. Sigworth. 1981. Improved patch-clamp techniques for high resolution current recording from cells and cell-free membrane patches. *Pflügers Arch. Eur. J. Physiol.* 391:85–100.

Helman, S.I., and N.K. Kizer. 1990. Apical sodium ion channels of tight epithelia as viewed from the perspective of noise analysis. *Curr. Top. Membr.* 37:117–155.

Hodgkin, A.L., and B. Katz. 1949. The effect of sodium ions on the electrical activity of the giant axon of the squid. *J. Physiol. (Camb.).* 108:37–77.

Holifield, B.F., and K. Jacobson. 1991. Mapping trajectories of Pgp-1 membrane protein patches on surfaces of motile fibroblasts reveals a distinct boundary separating capping on the lamella and forward transport on retracting tail. *J. Cell Sci.* 98: 191–203.

Kartner, N., J.W. Hanrahan, T.J. Jensen, A.L. Naismith, S. Sun, C.A. Ackerley, E.F. Reyes, L.-C. Tsui, J.M. Rommens, C.E. Bear, and J.R. Riordan. 1991. Expression of the cystic fibrosis gene in nonepithelial invertebrate cells produces a regulated anion conductance. *Cell.* 64:681–691.

Klaiber, K., N. Williams, T.M. Roberts, D.M. Papazian, L.Y. Jan, and C. Miller. 1990. Functional expression of *Shaker* K^+ channels in a Baculovirus-infected insect cell line. *Neuron.* 5:221–226.

Kusumi, A., Y. Sako, and M. Yamamoto. 1993. Confined lateral diffusion of membrane receptors as studied by single particle tracking (nanovid microscopy). Effects of calcium-induced differentiation in cultured epithelial cells. *Biophys. J.* 65:2021–2040.

Larsen, E.H., J. Fullton, M.J. Stutts, R.C. Boucher, and E.M. Price. 1992. Kinetics of Cl^- currents of *Sf*9 cells infected with human CFTR. *Pediatr. Pulmonol.* 267(Suppl. 8):119. (Abstr.)

Larsen, E.H., S.E. Gabriel, J. Fullton, R.C. Boucher, E. Price, and M.J. Stutts. 1993. Multiple single channel conductances and gating time constants of CFTR-mediated chloride currents. *FASEB J.* 7:A426:2468. (Abstr.)

Larsen, E.H., and B. Harvey. 1994. Chloride currents of single mitochondria-rich cells of toad skin epithelium. *J. Physiol. (Camb.).* 478:7–15.

Lindemann, B. 1984. Analysis of additively contaminated Lorentzians by integration. *Biophys. J.* 46:409–411.

Lindemann, B., and W. Van Driessche. 1978. The mechanism of Na-uptake through Na-selective channels in the epithelium of frog skin. *In* Membrane Transport Processes. Vol. 1. J.F. Hoffman, editor. Raven, New York. 155–178.

Marty, A., and E. Neher. 1995. Tight-seal whole-cell recording. *In* Single Channel Recording. B. Sakmann and E. Neher, editors. Plenum Press, New York. 31–52.

Mazzanti, M., L.J. DeFelice, and Y.-M. Liu. 1991. Gating of L-type Ca^{2+} channels in embryonic chick ventricle cells: dependence on voltage, current and channel density. *J. Physiol. (Camb.).* 443:307–334.

Neher, E. 1991. Correction for liquid junction potentials. *Methods Enzymol.* 207:123–131.

Neher, E., and C.F. Stevens. 1977. Conductance fluctuations and ionic pores in membranes. *Annu. Rev. Biophys. Bioeng.* 6:345–381.

Nielsen, C., L. Thomsen, M. Nielsen, S.E. Westh-Hansen, R.M. Witt, P.B. Rasmussen, S. Hastrup, and E.H. Larsen. 1995. Multiple versus single conductance states in $\alpha_3\beta_2\gamma_{2S}$ and $\alpha_3\beta_2$ members of the $GABA_A$ receptor family. *FASEB J.* 9:A390; 2258. (Abstr.)

Parker, J.C., and P.B. Dunham. 1989. Passive cation transport *In* Red Blood Cell Membranes. P. Agre and J.C. Parker, editors. Marcel Dekker, Inc., New York. 507–561.

Poussart, D.J.M. 1971. Membrane current noise in lobster axon under voltage clamp. *Biophys. J.* 11:211–234.

Sako, Y., and A. Kusumi. 1994. Compartmentalized structure of the plasma membrane for receptor movements as revealed by nanometer-level motion analysis. *J. Cell Biol.* 125:1251–1264.

Sarkadi, B., D. Bauzon, W.R. Huckle, H.S. Earp, A. Berry, H. Sushindran, E.M. Price, J.C. Olsen, R.C. Boucher, and G.A. Scarborough. 1992. Biochemical characterization of the cystic fibrosis transmembrane conductance regulator in normal and cystic fibrosis epithelial cells. *J. Biol. Chem.* 267:2987–2095.

Sten-Knudsen, O. 1978. Passive transport processes. *In* Membrane Transport in Biology. Concepts and Models. G. Giebisch, D.C. Tosteson, and H.H. Ussing, editors. Springer-Verlag, New York. 5–113.

Stevens, C.F. 1972. Inferences about membrane properties from electrical noise measurements. *Biophys. J.* 12:1028–1047.

Van Driessche, W., and W. Zeiske. 1985. Ion channels in epithelial membranes. *Physiol. Rev.* 65:833–903.